Site U1312–U1315 methods[1]

Expedition 306 Scientists[2]

Chapter contents

Introduction

Site locations

At all Expedition 306 sites, Global Positioning System (GPS) coordinates from precruise site surveys were used to position the vessel on site. The only seismic system used during the cruise was the 3.5 kHz profiler, which was monitored on the approach to each site to compare the seismic characteristics of the sediments with those from the precruise survey. Once the vessel was positioned at a site, the thrusters were lowered and a reference beacon was deployed. Although the automated stationkeeping system of the vessel usually uses GPS data, the beacon provides a backup reference in case of problems with the transmission of satellite data. The final site position was the mean position calculated from the GPS data collected over the time that the site was occupied.

Drilling operations

The advanced piston corer (APC) was the only coring system used during Expedition 306. The APC is a "cookiecutter" type system that cuts soft sediment cores with minimal coring disturbance relative to other Integrated Ocean Drilling Program (IODP) coring systems. The drill pipe is pressured up until the failure of two shear pins that hold the inner barrel attached to the outer barrel. The inner barrel advances into the formation and cuts the core. The driller can detect a successful cut, or "full stroke," from the pressure gauge on the rig floor.

The standard bottom-hole assembly (BHA) used at all Expedition 306 sites comprised an 11⅞ inch rotary bit, a bit sub, a seal bore drill collar, a landing saver sub, a modified top sub, a modified head sub, a nonmagnetic drill collar, four 8¼ inch drill collars, a tapered drill collar, six joints of 5½ inch drill pipe, and one crossover sub. A lockable float valve was used instead of the standard float assembly if the possibility of logging existed. APC refusal is conventionally defined in two ways: (1) the piston fails to achieve a complete stroke (as determined from the pump pressure reading) because the formation is too hard and (2) excessive force (>60 klb) is required to pull the core barrel out of the formation. In the case where full or partial stroke can be achieved but excessive force cannot retrieve the barrel, the core barrel can be "drilled over" (i.e., after the inner core barrel is successfully shot into the formation, the rotary bit is advanced to total depth to free the APC barrel). This strategy allows a hole to be advanced much far-

[1] Expedition 306 Scientists, 2006. Site U1312–U1315 methods. *In* Channell, J.E.T., Kanamatsu, T., Sato, T., Stein, R., Alvarez Zarikian, C.A., Malone, M.J., and the Expedition 303/306 Scientists. *Proc. IODP,* 303/306: College Station TX (Integrated Ocean Drilling Program Management International, Inc.). doi:10.2204/iodp.proc.303306.110.2006
[2] Expedition 306 Scientists' addresses.

doi:10.2204/iodp.proc.303306.110.2006

ther with the APC, the preferred coring tool. Nonmagnetic core barrels were used during all conventional APC coring. When utilizing the drillover technique, standard steel core barrels were used because they are more robust.

Each cored interval was ~9.5 m long, which is the length of a core barrel. In some cases, the drill string was drilled or "washed" ahead without recovering sediments to advance the drill bit to a target depth where core recovery needed to be resumed. Such advances were necessary in multiple holes at a site to ensure that coring gaps in one hole were covered by cored intervals in adjacent holes. The amount of advance was typically 1–4 m and accounted for drilling depth shift caused by tides, heave, and other factors (see also **"Stratigraphic correlation"**). Drilled and cored intervals are referred to in meters below rig floor (mbrf), which is measured from the dual elevator stool (DES) on the rig floor to the bottom of the drill pipe. In cases where sediments of substantial thickness cover the seafloor (as at all sites during Expedition 306), the mbrf depth of the seafloor is determined with a mudline core, assuming 100% recovery for the cored interval in the first core. If the first core recovered a full barrel of sediment (it probably "missed the mudline"), the seafloor reference depth of a previous or later hole was used. Water depth was calculated by subtracting the distance between the DES and sea level (typically 10–11 m, depending on the ship's load at a given time) from the mbrf depth. The water depth determined from this drill string measurement usually differs from precision depth recorder measurements by a few to several meters. The meters below seafloor (mbsf) depths of core tops are calculated by subtracting the seafloor depth in mbrf from the core top depth in mbrf. The core-top datums from the driller are the ultimate depth reference for any further depth calculation procedures.

Core handling and analysis

As soon as cores arrived on deck, headspace samples were taken using a syringe for immediate hydrocarbon analysis as part of the shipboard safety and pollution prevention program. Core catcher samples were taken for biostratigraphic analysis. When the core was cut in sections, whole-round samples were taken for shipboard interstitial water examinations. In addition, headspace gas samples were immediately taken from the ends of cut sections and sealed in glass vials for light hydrocarbon analysis.

Before splitting, whole-round core sections were run through the multisensor track (MST) and thermal conductivity measurements were taken. In addition, most whole cores were run through a "Fast Track" magnetic susceptibility core logger (MSCL) equipped with two magnetic susceptibility loops to facilitate real-time drilling decisions to maximize stratigraphic overlap between holes (see **"Stratigraphic correlation"**). The cores were then split into working and archive halves, from bottom to top, so investigators should be aware that older material could have been transported upward on the split face of each section. The working half of each core was sampled for both shipboard analysis (i.e., physical properties, carbonate, and bulk X-ray diffraction [XRD] mineralogy) and shore-based studies. Shipboard sampling was kept at a minimum during Expedition 306 to allow construction of a detailed sampling plan after the composite section was built. The archive-half sections were scanned on the digital imaging system (DIS), measured for color reflectance on the archive multisensor track (AMST), described visually and by means of smear slides, run through the cryogenic magnetometer, and finally photographed with color film a whole core at a time. Digital close-up photographs were taken of particular features for illustrations in site summary reports, as requested by scientists. Both halves of the core were then put into labeled plastic tubes, sealed, and transferred to cold storage space aboard the ship. At the end of the expedition, the cores were transferred from the ship into refrigerated trucks and then to cold storage at the IODP Bremen Core Repository in Bremen, Germany.

Curatorial procedures and sample depth calculations

Numbering of sites, holes, cores, and samples followed the standard IODP procedure. A full curatorial identifier for a sample consists of the following information: expedition, site, hole, core number, core type, section number, and interval in centimeters measured from the top of the core section. For example, a sample identification of "306-U1312A-1H-1, 10–12 cm" represents a sample removed from the interval between 10 and 12 cm below the top of Section 1 of Core 1 ("H" designates that this core was taken with the APC system) of Hole U1312A during Expedition 306. The "U" preceding hole numbers indicates the hole was drilled by the United States Implementing Organization (USIO) platform. Cored intervals are also referred to in "curatorial" mbsf. The mbsf of a sample is calculated by adding the depth of the sample below the section top and the lengths of all higher sections in the core to the core-top datum measured with the drill string. A soft to semisoft sediment core from less than a few hundred meters below seafloor expands upon recovery (typically a few percent to as much as 15%), so the recovered interval

does not match the cored interval. In addition, a coring gap typically occurs between cores, as shown by composite depth construction (i.e., some cored interval was lost during recovery or was never cut) (see **"Stratigraphic correlation"**). Thus, a discrepancy exists between the drilling mbsf and the curatorial mbsf. For instance, the curatorial mbsf of a sample taken from the bottom of a core is deeper than that from a sample from the top of the subsequent core, where the latter does correspond to the drilled core-top datum. During Expedition 306, multiple APC holes (typically three) were drilled at a site to construct a continuous composite section. This resulted in a meters composite depth (mcd) scale for each site that accommodates core expansion and drilling gaps through interhole correlation of closely spaced measurements of core physical properties (see **"Stratigraphic correlation"**).

Lithostratigraphy

This section outlines the procedures used to document the basic sedimentology of the deposits recovered during Expedition 306, including visual core description, smear slide description, digital color imaging, color spectrophotometry, and XRD studies. For consistency of Expedition 303 and 306 sediment classifications, the procedures described in the **"Site U1302–U1308 methods"** chapter were mainly followed. Only general procedures are outlined, except where they depart significantly from Ocean Drilling Program (ODP) and IODP conventions.

Sediment classification

The sediments recovered during Expedition 306 were composed of biogenic and siliciclastic components. They were described using the classification scheme of Mazzullo et al. (1988). The biogenic component is composed of the skeletal debris of open-marine calcareous and siliceous microfauna (e.g., foraminifers and radiolarians, respectively) and microflora (e.g., calcareous nannofossils and diatoms, respectively) and associated organisms. The siliciclastic component is composed of mineral and rock fragments derived from igneous, sedimentary, and metamorphic rocks. The relative proportions of these two components are used to define the major classes of "granular" sediments in the scheme of Mazzullo et al. (1988).

The lithologic names assigned to these sediments consist of a principal name based on composition, degree of lithification, and/or texture as determined from visual description of the cores and from smear slide observations. The total calcium carbonate content of the sediments, determined on board (see **"Geochemistry"**), was also used to aid in classification. For a sediment that is a mixture of components, the principal name is preceded by major modifiers (in order of increasing abundance) that refer to components making up ≥25% of the sediment. Minor components that represent between 10% and 25% of the sediment follow the principal name (after a "with") in order of increasing abundance. Minor sedimentary components <10% in abundance are not reflected in the lithologic name. For example, an unconsolidated sediment containing 30% nannofossils, 50% clay minerals, 15% foraminifers, and 5% quartz would be described as a nannofossil clay with foraminifers. For biogenic sediments (i.e., >50% biogenic grains; see below), major or minor modifiers of siliciclastic components were summed, resulting in a more inclusive/general term for the name of the sediment. For example, an unconsolidated sediment containing 55% nannofossils, 15% foraminifers, 10% clay minerals, 10% quartz, and 10% detrital calcite would be described as a silty clay nannofossil ooze with foraminifers. Minor sedimentary components are not designated in the Graphic Lithology column of the barrel sheets.

These naming conventions follow the ODP sediment classification scheme (Mazzullo et al., 1988), with the exception that during Expedition 306 a separate "mixed sediment" category was not distinguished (Fig. **F1**). As a result, biogenic sediments are those that contain >50% biogenic grains and <50% siliciclastic grains, whereas siliciclastic sediments are those that contain >50% siliciclastic grains and <50% biogenic grains. For the classification of biogenic carbonate oozes, three categories were used:

- Foraminifer ooze (content of foraminifers >50%).
- Nannofossil ooze (content of nannofossils >50%).
- Calcareous ooze (content of nannofossils + foraminifers >50%, but content of nannofossils <50% and content of foraminifers <50%).

Some sediments contained >50% biogenic components, but no single biogenic component was >50%. In these instances, the siliceous and calcareous components were summed, resulting in a lithologic name that reflects the relative contribution of each biogenic component by listing these components in order of increasing abundance. For example, an unconsolidated sediment containing 45% nannofossils, 15% diatoms, 10% sponge spicules, 10% clay minerals, 10% quartz, and 10% detrital calcite would be described as a silty clay biosiliceous-nannofossil ooze.

Size divisions for siliciclastic grains are those of Wentworth (1922) (Fig. F2), with 10 major textural categories defined on the basis of the relative proportions of sand, silt, and clay (Fig. F3); however, distinguishing between some of these categories is difficult (e.g., silty clay versus clayey silt) without accurate measurements of grain size abundances. For siliciclastic sediments, the term "clay" is only used to describe particle size and is applied to both clay minerals and other siliciclastic/detrital mineral components <4 µm in size. Size-textural qualifiers were not used for biogenic sediment names (e.g., nannofossil clay implies that the dominant component is detrital clay rather than clay-sized nannofossils).

During Expedition 306, neritic and chemical sediments were not encountered except as accessory components; therefore, these categories are not addressed below. Sediments containing >50% silt- and sand-sized volcanic grains were classified as ash layers.

Terms that describe lithification vary depending upon the dominant composition as described below:

- Sediments composed predominantly of calcareous pelagic organisms (e.g., nannofossils and foraminifers): the lithification terms "ooze" and "chalk" reflect whether the sediment can be deformed with a finger (ooze) or can be scratched easily by a fingernail (chalk).
- Sediments composed predominantly of siliceous microfossils (diatoms, radiolarians, and siliceous sponge spicules): the lithification terms "ooze" and "diatomite/radiolarite/spiculite" reflect whether the sediment can be deformed with a finger (ooze) or cannot be easily deformed manually (diatomite/radiolarite/spiculite).
- Sediments composed predominantly of siliciclastic material: if the sediment can be deformed easily with a finger, no lithification term is added, and the sediment is named for the dominant grain size (e.g., "clay"). For more consolidated material, the lithification suffix "-stone" is appended to the dominant size classification (e.g., "claystone").
- Sediments composed of sand-sized volcaniclastic grains: if the sediment can be deformed easily with a finger, the interval is described as ash. For more consolidated material, the rock is called tuff.

Visual core description

Preparation for core description

The standard method of splitting a core by pulling a wire lengthwise through its center tends to smear the cut surface and obscure fine details of lithology and sedimentary structure. When necessary during Expedition 306, the archive halves of cores were gently scraped across, rather than along, the core section using a stainless steel or glass scraper to prepare the surface for unobscured sedimentologic examination and digital imaging. Scraping parallel to bedding with a freshly cleaned tool prevented cross-stratigraphic contamination.

Sediment barrel sheets

Core description forms, or "barrel sheets," provide a summary of the data obtained during shipboard analysis of each sediment core. Detailed observations of each section were recorded initially by hand on standard IODP visual core description (VCD) forms. Copies of original VCD forms are available from IODP upon request. This information was subsequently entered into AppleCORE (version 9.4), which generates a simplified annotated graphical description (barrel sheet) for each core (Fig. F4). Site, hole, and depth (in mbsf or mcd if available) are given at the top of the barrel sheet, with the corresponding depths of core sections along the left margin. Columns on the barrel sheets include Graphic Lithology, Bioturbation, Structures, Accessories, Sediment Disturbance, Sample Types, Color, and Description. These columns are discussed in more detail below.

Graphic lithology

Lithologies of the core intervals recovered are represented on barrel sheets by graphic patterns in the Graphic Lithology column using the symbols illustrated in Figure F5. A maximum of two different lithologies (for interbedded sediments) or three different components (for a uniform sediment) can be represented within the same core interval. Minor lithologies, present as thin interbeds within the major lithology, are shown by a dashed vertical line dividing the lithologies. Lithologic abundances are rounded to the nearest 10%. Lithologies that constitute <25% of the core are generally not shown but are listed in the Lithologic Description section. However, some distinctive minor lithologies, such as ash layers, are included graphically in the lithology column. Contact types (e.g., sharp, scoured, gradational, and bioturbated) are also shown in the Graphic Lithology column. Relative abundances of lithologies reported in this way are useful for general characterization of the sediment but do not constitute precise, quantitative observations.

Bioturbation

For bioturbation classification, five levels of bioturbation were used during Expedition 306. These levels are illustrated with graphic symbols in the

Bioturbation column (Fig. F6), and are presented in a scheme based on Droser and Bottjer (1986) (Fig. F7). Bioturbation intensity is classified as:

- Strong (>50%),
- Moderate (10%–50%),
- Rare (<10%), and
- Absent (no bioturbation).

Most of the Expedition 306 sediments fall into one of these four categories. As a fifth category, the classification "homogeneous" occasionally was used to represent a totally bioturbated or homogenized sediment. Note, however, that in a homogeneous sediment section with no color changes at all it is often not clearly possible to estimate the degree of bioturbation, which may range from absent to totally bioturbated or homogenized.

Sedimentary structures

The locations and types of sedimentary structures visible on the prepared surfaces of the split cores are shown in the Structure column of the core description form using the symbols represented in Figure F6. Symbols in this column indicate the locations of individual bedding features and any other sedimentary features, such as scours, ash layers, ripple laminations, and fining-upward or coarsening-upward intervals.

Accessories

Lithologic, diagenetic, and paleontologic accessories, such as nodules, sulfides, and shells, are indicated in the Accessories column on the barrel sheets. The symbols used to designate these features are shown in Figure F6.

Sediment disturbance

Drilling-related sediment disturbance that persists over intervals of ~20 cm or more is recorded in the Disturbance column using the symbols shown in Figure F6. The degree of drilling disturbance is described for soft and firm sediments using the following categories:

- Slightly disturbed: bedding contacts are slightly deformed.
- Moderately disturbed: bedding contacts have undergone extreme bowing.
- Extremely disturbed: bedding is completely deformed as flow-in, coring/drilling slurry, and other soft-sediment stretching and/or compressional shearing structures attributed to coring/drilling. The particular type of deformation may also be noted (e.g., flow-in, gas expansion, etc.).
- Soupy: intervals are water saturated and have lost all aspects of original bedding.

Sample types

Sample material taken for shipboard sedimentologic and chemical analysis consisted of pore water whole rounds, micropaleontology samples, smear slides, and discrete samples for XRD. Typically, one to five smear slides were made per core, one pore water sample was taken at a designated interval, and a micropaleontology sample was obtained from the core catcher of most cores. XRD samples were taken only where needed to assess the lithologic components. Additional samples were selected to better characterize lithologic variability within a given interval. Tables summarizing relative abundance of sedimentary components from the smear slides were generated using a spreadsheet exported from a standard program (Sliders) used during the cruise.

Color

Color is determined qualitatively using Munsell Soil Color Charts (Munsell Color Company, 1994) and described immediately after cores are split to avoid color changes associated with drying and redox reactions. When portions of the split core surface required cleaning with a stainless steel or glass scraper, this was done prior to determining the color. Munsell color names are provided in the Color column on the barrel sheet, and the corresponding hue, value, and chroma data are provided in the Description column.

Description

The written description for each core contains a brief overview of both major and minor lithologies present and notable features such as sedimentary structures and disturbances resulting from the coring process.

Smear slides

Smear slide samples were taken from the archive halves during core description. For each sample, a small amount of sediment was removed with a wooden toothpick, dispersed evenly in deionized water on a 1 inch × 3 inch glass slide, and dried on a hot plate at a low setting. A drop of mounting medium and a 1 inch × 1 inch cover glass was added, and the slide was placed in an ultraviolet light box for ~30 min. Once fixed, each slide was scanned at 100×–200× with a transmitted light petrographic microscope using an eyepiece micrometer to assess grain-size distributions in clay (<4 µm), silt (4–63 µm), and sand (>63 µm) fractions. The eyepiece mi-

crometer was calibrated once for each magnification and combination of ocular and objective using an inscribed stage micrometer.

Relative proportions of each grain size and type were estimated by microscopic examination. Note that smear slide analyses tend to underestimate the abundance of sand-sized and larger grains (e.g., foraminifers, radiolarians, and siliciclastic sand) because these are difficult to incorporate into the smear. Clay-sized biosilica, being transparent and isotropic, is also very difficult to quantify. Clay minerals, micrite, and nannofossils can also be difficult to distinguish at the very finest (less than ~4 µm) size range. After scanning for grain-size distribution, several fields were examined at 200×–500× for mineralogical and microfossil identification. Standard petrographic techniques were employed to identify the commonly occurring minerals and biogenic groups as well as important accessory minerals and microfossils.

Smear slide analysis data tables are included in **"Core descriptions."** These tables include information about the sample location, whether the sample represents a dominant (D) or a minor (M) lithology in the core, and the estimated percentages of sand, silt, and clay together with all identified components. Relative abundances of different grain types below 5% were assigned on a semiquantitative basis using the following abbreviations: tr = trace (0%–1%), and R = rare (1%–5%).

Abundance of gravel-sized grains

One of the primary objectives of Expeditions 303 and 306 was to collect cores that record the paleoclimatic history of the North Atlantic at millennial and longer timescales. Because of the geographic location and the geologic age of these sediments, ice-rafted debris (IRD) was expected to be an important part of that paleoclimatic record. The most easily identified IRD consists of outsized clasts in a fine-grained pelagic matrix and is often defined operationally as gravel-sized grains. During Expedition 306, the abundance of IRD was estimated by counting the number of gravel-sized grains (i.e., granule size and larger) in each 1 cm increment of the core. Wherever possible, composition, size, and angularity of each clast were also determined. All of this information is recorded in a table within each site chapter.

Spectrophotometry (color reflectance)

Reflectance of visible light from the surface of split sediment cores was routinely measured using a Minolta spectrophotometer (model CM-2002) mounted on the AMST. The AMST measures the archive half of each core section and provides a high-resolution stratigraphic record of color variations for visible wavelengths (400–700 nm). Freshly split soft cores were covered with clear plastic wrap and placed on the AMST. Measurements were taken at 2.0 cm spacing. The AMST skips empty intervals and intervals where the core surface is well below the level of the core liner but does not skip relatively small cracks, disturbed areas of core, or large clasts. Thus, AMST data may contain spurious measurements, which should be edited out of the data set. Each measurement recorded consists of 31 separate determinations of color reflectance in 10 nm wide spectral bands from 400 to 700 nm. Additional detailed information about measurement and interpretation of spectral data with the Minolta spectrophotometer can be found in Balsam et al. (1997, 1998) and Balsam and Damuth (2000).

Digital color imaging

Systematic high-resolution line scan digital core images of the archive half of each core were obtained using the Geotek X-Y DIS (Geoscan II). This DIS collects digital images with three line-scan charge-coupled device arrays (1024 pixels each) behind an interference filter to create three channels (red, green, and blue). The image resolution is dependent on the width of the camera and core. The standard configuration for the Geoscan II produces 300 dpi on an 8 cm wide core with a zoom capability up to 1200 dpi on a 2 cm wide core. Synchronization and track control are better than 0.02 mm. The dynamic range is 8 bits for all three channels. The FrameStore card has 48 MB of onboard random-access memory for the acquisition of images with an Industry Standard Architecture interface card for personal computers. After cores were visually described, they were placed in the DIS and scanned. A spacer holding a neutral gray color chip and a label identifying the section was placed at the base of each section and scanned along with each section. Output from the DIS includes a Windows bitmap (.BMP) file and a JPEG (.JPEG, .JPG) file for each section scanned. The bitmap file contains the original data. Additional postprocessing of data was done to achieve a medium-resolution JPEG image of each section and a composite JPEG image of each core, which is comparable to the traditional photographic image of each core. The JPEG image of each section was produced by an Adobe Photoshop batch job that opened the bitmap file, resampled the file to a width of 0.6 inch (~15 mm) at a resolution of 300 pixels/inch, and saved the result as a maximum-resolution JPEG. The DIS was calibrated for black and white

approximately every 12 h. No significant change in this calibration was observed during Expedition 306. A constant aperture setting of f/11 was used.

X-ray diffraction analysis

Selected samples were taken for qualitative mineral analysis by using an XRD Philips model PW1729 X-ray diffractometer using Ni-filtered CuK_{α} radiation. Instrument conditions were as follows: 40 kV, 35 mA; goniometer scan from 2° to 70°2θ (air-dried samples) and from 2° to 12°2θ (glycolated samples); step size = 0.01°2θ; scan speed = 1.2°2θ/min; and count time of 0.5 s. Some samples were decalcified using 10% acetic acid then washed repeatedly with demineralized water in a centrifuge. The carbonate-free fraction was deflocculated with a 1% Calgon (sodium hexametaphosphate) solution and homogenized in a sonic dismembrator for 1 min. MacDiff software (version 4.1.1 PPC by Rainer Petschick) was used to display diffractograms, and identifications are based on multiple peak matches using the mineral database provided with MacDiff. Diffractograms were peak corrected to match the calcite peak at 3.035 Å. In the absence of calcite, no peak correction was applied.

Biostratigraphy

Preliminary ages were assigned primarily based on core catcher samples. Samples from within the cores were examined when a more refined age determination was necessary. Ages for calcareous nannofossil, foraminifer, diatom, and radiolarian events from the late Miocene–Quaternary were estimated by correlation to the geomagnetic polarity timescale (GPTS) of Cande and Kent (1995). The biostratigraphic events, zones, and subzones for nannofossils, planktonic foraminifers, diatoms, and radiolarians are summarized in Figure **F8.** The Pliocene/Pleistocene boundary has been formally located just above the top of the Olduvai (C2n) magnetic polarity subchronozone (Aguirre and Pasini, 1985) and just below the lowest occurrence of *Gephyrocapsa caribbeanica* at 1.73 Ma (Takayama and Sato, 1993–1995). *Gephyrocapsa* species occur in upper Pliocene sediments; however, medium-sized forms (>4 µm) first appear just above the Pliocene/Pleistocene boundary (de Kaenel et al., 1999), coincident with the lowest occurrence of *G. caribbeanica* (Takayama and Sato, 1993–1995; Sato et al., 1999). Thus, we define *G. caribbeanica* and *Gephyrocapsa oceanica* as specimens >4 µm to distinguish between Pliocene and Pleistocene forms. In addition, the first occurrences (FOs) of *Globorotalia truncatulinoides* and *Globorotalia inflata* at 2.09 Ma immediately below the Olduvai subchronozone is very useful to approximate the Neogene/Quaternary boundary. Thus for this study, we locate the Pliocene/Pleistocene boundary between the FO of *G. caribbeanica* (>4 µm) and the FOs of *G. truncatulinoides* and *G. inflata*.

The Miocene/Pliocene boundary has not yet been formally defined. Its location is not well constrained because no biostratigraphic event has been identified in this interval of time; however, the last occurrence (LO) of *Discoaster quinqueramus is* at 5.5 Ma and the FO of *Thalassiosira convexa* is between 6.1 and 6.4 Ma.

Details of the shipboard methods are described below for each microfossil group.

Calcareous nannofossils

The zonal scheme established by Martini (1971) was used for Miocene–Quaternary sequences during Expedition 306. In addition, the late Pliocene–Quaternary biostratigraphic horizons defined by Sato et al. (1999) were used for more detailed correlations. Correlation of the zonal scheme and biostratigraphic horizons to the GPTS of Cande and Kent (1995) is shown in Figure **F8.** Age estimates for datums tied to the geomagnetic timescale are also shown in Figure **F8** and listed in Table **T1.**

Methods

Samples were prepared utilizing standard smear slide methods with Norland optical adhesive as a mounting medium. Calcareous nannofossils were examined with a Zeiss light microscope at 1250× magnification using cross-polarized light, transmitted light, and phase contrast light.

We followed the taxonomic concepts summarized in Takayama and Sato (1987; Deep Sea Drilling Project [DSDP] Leg 94). Calcareous nannofossil preservation was assessed as follows:

- G = good (little or no evidence of dissolution or overgrowth, little or no alteration of primary morphological features, and specimens are identifiable to the species level).
- M = moderate (minor dissolution or crystal overgrowth observed, some alteration of primary morphological features, but most specimens are identifiable to the species level).
- P = poor (strong dissolution or crystal overgrowth, significant alteration of primary morphological features, and many specimens are unidentifiable at the species and/or generic level).

The total abundance of calcareous nannofossils for each sample was estimated as follows:

V = very abundant (>100 specimens per field of view [FOV]).
A = abundant (11–100 specimens per FOV).
C = common (1–10 specimens per FOV).
F = few (1 specimen per 2–10 FOVs).
R = rare (1 specimen per 11 or more FOVs).
B = barren.

Nannofossil abundances of individual species were recorded as follows:

A = abundant (11 or more specimens per FOV).
C = common (1–10 specimens per FOV).
F = few (1 specimen per 2–10 FOVs).
R = rare (1 specimen per 11 or more FOVs).
P = present, but abundance was not quantitatively determined.
? = questionable occurrence.
* = reworked occurrence.

Foraminifers

Preliminary ages were assigned based on the occurrence of planktonic foraminifers from core catcher samples. Stratigraphic events of Weaver and Clement (1987) for the North Atlantic and Lourens et al. (1996) for the Mediterranean were applied to the Pliocene and Pleistocene samples of Expedition 306 (Fig. F8). For the late Miocene, however, planktonic foraminiferal events as defined by Sierro et al. (1993, 2001), Krijgsman et al. (1995), and Hilgen et al. (2000) for the northeast Atlantic and Mediterranean Sea were used (Table T2). Middle Miocene stratigraphy is based on Spezzaferri (1998). The species identified as *Globorotalia* cf. *crassula* by Weaver and Clement (1987) has a highly convex dorsal side, which led us to relate this species to *Globorotalia hirsuta* during Expedition 306. Consequently, only *G. hirsuta* is listed in the tables and the LO of *G.* cf. *crassula*, dated at 3.18 Ma by Weaver and Clement (1987), is renamed to "disappearance of *G. hirsuta*." *Globorotalia conomiozea* and *Globorotalia miotumida* have been grouped together as the *G. miotumida* group. For the abundance estimates, *Neogloboquadrina acostaensis* is combined with *Neogloboquadrina pachyderma*, and in the Miocene the *Globorotalia menardii* group also includes *Globorotalia plesiotumida* and *Globorotalia merotumida* following Sierro et al. (1993). Otherwise, taxonomic concepts for Neogene taxa are adopted from Kennett and Srinivasan (1983). The magnetic stratigraphy for the Cenozoic is derived from Cande and Kent (1995).

The benthic foraminifers are defined by assemblage zones. Boundaries are placed at major shifts in the fauna. Each zone is named after its dominant species. Benthic foraminifers provide limited biostratigraphic age control as currently applied to Expedition 306 samples. Whenever possible, the genus *Stilostomella* was used as a marker because most of its species disappeared from the global ocean at different latitudes during the interval of 1.0–0.6 Ma (Hayward, 2001). Taxonomic assignments on the generic level follow Loeblich and Tappan (1988). Benthic foraminifers were identified mainly to determine past changes in oceanographic conditions and surface water productivity. Oxygenation and carbon flux are the main factors controlling abundance and species composition in deep-sea assemblages (Jorissen et al., 1995; Altenbach et al., 2003).

During the benthic assemblage analysis, the presence or absence of ostracodes was noted, as they will be used for postcruise paleoceanographic studies.

Methods

From each core catcher, 20 cm^3 of sediment was analyzed for planktonic and benthic foraminifers. Unlithified sediment samples were soaked in tap water and then washed over a 63 µm sieve. Semilithified material was soaked in a 3% H_2O_2 solution before washing. Washed samples were dried at 60°C and analyzed under a ZEISS Stemi SV11 or ZEISS DR binocular microscope. The residue was split, with three-quarters of the sample being used for the benthic and one-quarter for the planktonic foraminifers analysis. Sieves for wet sieving were cleaned in a sonicator for several minutes and for dry sieving were blown out with compressed air to avoid contamination between successive samples.

Planktonic foraminifer abundance in the fraction >125 µm in relation to the total residue was categorized as follows:

D = dominant (>30%).
A = abundant (10%–30%).
F = few (5%–10%).
R = rare (1%–5%).
P = present (<1%).
B = barren.

Benthic foraminifer abundance in a sample of the >63 µm size fraction is registered as follows:

D = dominant (>30%).
A = abundant (10%–30%).
F = few (5%–10%).
R = rare (1%–5%).
P = present (<1%).
B = barren.

Preservation includes the effects of diagenesis, epigenesis, abrasion, encrustation, and/or dissolution. Preservation of planktonic and benthic species was categorized as follows:

VG = very good (no evidence of breakage or dissolution).

G = good (dissolution effects are rare; >90% of specimens unbroken).
M = moderate (dissolution damages, such as etched and partially broken tests, occur frequently; 30%–90% of specimens unbroken).
P = poor (strongly recrystallized or dominated by fragments or corroded specimens).

Diatoms

Except for previous Leg 94 and ODP Leg 162, diatom data from the mid-latitude North Atlantic Ocean are sparse, and only a few diatom biostratigraphic studies have been completed. The Neogene and Quaternary diatom zonation used for the high-latitude sites of Expedition 306 is that proposed by Baldauf (1984) and Koç et al. (1999). The late Miocene–Holocene portion of this zonation is based on the occurrence in the North Atlantic of a warm-temperature diatom assemblage similar to that recorded from the eastern equatorial Pacific (Burckle, 1972, 1977; Baldauf, 1984; Barron, 1985). In addition, diatom stratigraphies from the Japan Trench (Akiba and Yanagisawa, 1986), as well as from the North Pacific–Bering Sea region (Koizumi, 1971) were adopted in an attempt to cover the gap in the late Miocene–late Pliocene high-latitude North Atlantic diatom stratigraphy (Koç et al., 1999). This is partly justified by the rare possible finding of *Neodenticula kamtschatica* during Expedition 303 (see **"Biostratigraphy"** in "Site U1302–U1308 methods"). Figure **F8** lists diatom biostratigraphic events, paleomagnetic calibration, and age estimates used during this expedition.

Typical diatom assemblages preserved in the sedimentary record can be used as tracers for the corresponding hydrographic conditions in the surface waters. Diatoms characterize fertile surface waters of high latitudes and coastal upwelling areas. In the North Atlantic north of ~50°N, they are diverse and are the main contributors to the biogenic silica preserved in the sediment (Baldauf, 1984; Koç et al., 1999).

Methods

Two types of slides were prepared for diatom analysis depending on overall abundance. For intervals of high abundance, smear slides were prepared from a small amount of raw material from the core catcher. When dictated by a low concentration of diatom valves and/or abundant clay, selected core catcher samples were processed by boiling in a solution of H_2O_2 and sodium pyrophosphate to remove organic matter and to disperse the clay-sized material followed by treatment with HCl to remove $CaCO_3$. The treated samples were then washed several times with distilled water. In each case, aliquots of raw and cleaned samples were mounted on microscope slides using Norland optical adhesive. All slides were examined with illumination at 1000× magnification for stratigraphic markers and paleoenvironmentally sensitive taxa. The counting convention of Schrader and Gersonde (1978) was adopted. Overall diatom abundance and species relative abundances were determined based on smear slide evaluation using the following conventions:

A = abundant (>100 valves per traverse).
C = common (40–100 valves per traverse).
F = few (20–40 valves per traverse).
R = rare (10–20 valves per traverse).
T = trace (2–9 valves per traverse).
T = single occurrence or fragment per tranverse.
B = barren.

For computing purposes, a number was assigned to each abundance category (0 = B, 1 = T, 2 = R, 3 = F, 4 = C, and 5 = A).

Preservation of diatoms was determined qualitatively as follows:

G = good (weakly silicified forms present and no alteration of frustules observed).
M = moderate (weakly silicified forms present, but with some alteration).
P = poor (weakly silicified forms absent or rare and fragmented, and the assemblage is dominated by robust forms).

A number was assigned to each category (1 = P, 2 = M, and 3 = G).

Radiolarians

There is currently no working high-resolution radiolarian biostratigraphic framework applicable to the North Atlantic, but several existing sites could potentially be used for this matter. The stratigraphic framework established by Goll and Bjørklund (1989) is only applicable for the Norwegian Sea. Goll and Bjørklund (1989) found that most radiolarians encountered in the Norwegian Sea are endemic and thus proposed a unique biostratigraphic scheme for that area. Lazarus and Pallant (1989) did not establish a biostratigraphic zonal scheme for the Labrador Sea, but as the species are clearly different from those in the Norwegian Sea, the biostratigraphic scheme of the Norwegian Sea cannot be used. Thus, there is no available radiolarian biostratigraphic framework for the Labrador Sea at present. On the other hand, Westberg-Smith and Riedel (1984) recognized two radiolarian zones, including the *Stichocorys peregrina* and *Sphaeropyle langii* Zones, for the late Miocene and early Pliocene in deep-sea cores from the Rockall Plateau, high-latitude North Atlantic. Haslett (1994, 2004) reported several radiolarian biostratigraphic

events throughout the Pliocene and Pleistocene at the mid-latitude North Atlantic DSDP Site 609, which is directly comparable to this expedition.

For the above reason, we will try to apply the scheme suggested by Haslett (1994, 2004), especially for the Pliocene–Pleistocene section, and Westberg-Smith and Riedel (1984) for the late Miocene and early Pliocene. Numerical age datums were tied to the GPTS of Cande and Kent (1995). Primary datums from late Miocene to Pleistocene are listed in Figure F8.

As mentioned above, radiolarians in the North Atlantic show a different faunal distribution than in the Norwegian Sea, the Labrador Sea, and the mid-latitude North Atlantic, making it difficult to establish a biostratigraphic framework in this region. However, radiolarian biostratigraphy of the North Atlantic will play an important role not only in a local biostratigraphic zonation, but also in the paleoceanographic reconstruction of this area. During preglacial times, oceanic conditions should have been more homogeneous in the North Atlantic and radiolarian associations have a better chance for a more uniform distribution. The hydrographical and ecological situations are more provincial in the postglacial period, so radiolarian associations should have been endemic to specific regions. Therefore, most likely, local biostratigraphic schemes have to be established in the Labrador Sea, the North Atlantic, and the Norwegian Sea, respectively.

Methods

Core catcher samples were treated with a 5%–8% solution of HCl to dissolve all calcareous components. The solution was sieved through a 45 µm mesh screen. The residue was disaggregated by gentle boiling in 5%–8% H_2O_2 with a few grams of Calgon and sieved again. After settling in the beaker, the residue was picked up and dropped on a slide using an eyedropper. The sample was spread with a toothpick and dried on a hot plate. A few drops of Norland optical adhesive were used to apply a 22 mm × 50 mm glass coverslip.

Overall radiolarian abundances were determined based on slide evaluation with a 20× objective lens using the following convention:

A = abundant (>100 specimens per traverse).
C = common (51–100 specimens per traverse).
F = few (11–50 specimens per traverse).
R = rare (1–10 specimens per traverse).
T = trace (<1 specimens per traverse).
B = barren.

The abundance of individual species was recorded relative to the fraction of the total assemblages as follows:

A = abundant (>10% of the total assemblage).
C = common (5%–10% of the total assemblage).
F = few (<5% of the total assemblage).
R = rare (a few or more specimens per slide).
T = trace (present in slide).
B = barren.

Preservation was recorded as follows:

G = good (majority of specimens complete, with minor dissolution, recrystallization, and/or breakage).
M = moderate (minor but common dissolution, with a small amount of breakage of specimens).
P = poor (strong dissolution, recrystallization, or breakage, many specimens unidentifiable).

The abundances of lithic grains, including tephra and organic compounds in the slides, were also evaluated.

Paleomagnetism

Paleomagnetic analyses during Expedition 306 consisted of long-core measurements of the natural remanent magnetization (NRM) of archive-half sections before and after alternating-field (AF) demagnetization. In addition, low-field volume magnetic susceptibility was measured on whole cores using the MSCL and MST devices.

NRM measurements and AF demagnetizations were performed using a three-axis (x, y, and z) long-core cryogenic magnetometer (2G Enterprises model 760-R). This instrument is equipped with a direct-current superconducting quantum interference device (DC-SQUID) and has an inline AF demagnetizer capable of reaching peak fields of 80 mT (2G Enterprises model 2G600). The spatial resolution measured by the width at half-height of the pickup coils response is <10 cm for all three axes, although they sense a magnetization over a core length up to 30 cm. The effective sensor length (i.e., area under the normalized SQUID response function) of axes x, y, and z are 6.071, 6.208, and 9.923 cm, respectively. Experiments conducted during ODP Legs 186 and 206 showed that the background noise level of the magnetometer is about ±2 × 10^{-9} Am^2 and that reliable measurements could be obtained for intensities greater than ~10^{-5} A/m for split-core sections (Shipboard Scientific Party, 2000, 2003b).

Archive halves of all core sections were measured unless precluded by drilling-related deformation. Measurements were made at intervals of 5 cm, starting

15 cm above the top and ending 15 cm below the base of each section. These additional data points were measured to allow deconvolution of the records in later shore-based studies. When performing shipboard data analyses (e.g., for site reports), data corresponding to the top and bottom 10 cm of each core section were edited to account for edge effects. The number of demagnetization steps used to remove the drill string magnetic overprint and isolate a useful magnetic moment reflected time constraints. A three-step demagnetization scheme consisting of 0 (NRM), 10, and 20 mT was used initially. When core flow through the laboratory needed to be increased, only the first (NRM) and last (20 mT) demagnetization steps were used, reducing the measurement time by ~5 min per core section. The use of peak AF demagnetization fields lower than 20 mT ensure that archive halves remain useful for shore-based studies.

Measurements were undertaken using the standard IODP magnetic coordinate system described in Figure **F9** (+x = vertical upward from the split surface of archive halves, +y = left-hand split surface when looking upcore, and +z = downcore). Data were stored using the standard IODP file format. Data were manually checked for quality, and the autosave option was not used. The sample interval was set to 5 cm, leader and trailer lengths were both set to 15 cm, and a drift correction was applied. The program options for skipping voids and gaps at the top of the section were not used. Void depths and otherwise disturbed intervals were instead manually noted on the "cryomag log sheets" and later taken into account. All sections were measured using an internal diameter setting of 6.5 cm. Background tray magnetization was measured at least once per shift (e.g., at the beginning of each shift) and subtracted from all measurements.

During APC coring a nonmagnetic "monel" core barrel was used for all but some overdrilled parts of the section (see **"Introduction"**). Full orientation was attempted using the Tensor orientation tool beginning at Core 3 of all holes when available. The Tensor tool is rigidly mounted onto a nonmagnetic sinker bar attached to the top of the core barrel assembly. The Tensor tool consists of three mutually perpendicular magnetic field fluxgate sensors and two perpendicular gravity sensors. The information from both sets of sensors allows the azimuth and dip of the hole to be measured as well as azimuth of the APC core (Shipboard Scientific Party, 2003a). The azimuthal reference line is the double orientation line on the core liner and remains on the working half after the core is split.

Where the shipboard AF demagnetization appears to have isolated the characteristic remanent magnetization, paleomagnetic inclinations and/or declinations of the highest demagnetization step, typically 20 mT, were used to define magnetic polarity zones. The revised timescale of Cande and Kent (1995) with updated age estimates for the Cobb Mountain (1.190–1.215 Ma) (Channell et al., 2002) and Reunion (2.115–2.153 Ma) (Channell et al., 2003) Subchronozones was used as a reference for the ages of correlative Cenozoic polarity chrons.

The magnetic susceptibility of whole-core sections was measured on two separate track systems. Whole-core sections were measured on a MSCL to rapidly acquire magnetic susceptibility data for stratigraphic correlation (see **"Stratigraphic correlation"**). After whole cores warmed to room temperature, measurements were made as part of the MST analyses (see **"Physical properties"**).

Stratigraphic correlation

Paleomagnetic and paleoclimatic objectives of Expedition 306 required the recovery of complete stratigraphic sections, yet stratigraphers have demonstrated that a continuous section is rarely recovered from a single ODP borehole because of core-recovery gaps between successive APC and extended core barrel cores despite 100% or more nominal recovery (Ruddiman et al., 1987; Hagelberg et al., 1995). Construction of a complete section, referred to as a composite splice, requires combining stratigraphic intervals from two or more holes cored at the same site. To maximize the probability of bridging core-recovery gaps in successive holes, the depths below the seafloor from which cores are recovered are offset between the holes. This practice ensures that most between-core intervals missing within a given hole are recovered in at least one of the adjacent holes. During Expedition 306, two or more holes were cored at all sites and used to construct composite sections.

Our composite sections and splice construction methodology follows one which has been successfully employed during a number of previous legs of the ODP (e.g., Hagelberg et al., 1992; Curry, Shackleton, Richter, et al., 1995; Jansen, Raymo, Blum, et al., 1996; Lyle, Koizumi, Richter, et al., 1997; Gersonde, Hodell, Blum, et al., 1999, Wang, Prell, Blum, et al., 2000; Mix, Tiedemann, Blum, et al., 2003; Zachos, Kroon, Blum, et al., 2004; among others) and, most recently, during Expedition 303 (see **"Composite section"** in the "Site U1308–U1311 methods" chapter). Assembly and verification of a complete composite stratigraphic section requires construction of a composite depth scale. Other depth scales (discussed below) can be implemented using downhole logging

data and/or combining splicing and drill pipe depths.

Once a composite depth scale has been completed, a stratigraphically continuous and complete composite splice can be created from representative intervals from the multiple holes. Ideally, both core-recovery gaps and intervals with coring deformation are absent in the spliced section. The continuity and completeness of the spliced section is dependent on avoiding coeval core-recovery gaps in the multiple holes, which can be done through real time adjustments to the depths at which a core is collected as discussed below.

Meters composite depth scale

The goal of constructing a composite depth scale is to place coeval, laterally continuous stratigraphic features into a common frame of reference by depth shifting the mbsf depth scales of individual cores to maximize correlation between holes. In the composite depth scale used by ODP and IODP, referred to as the mcd scale, the depths of the individual cores can only be shifted by a constant amount, without permitting expansion or contraction of the relative depth scale within any core. Ultimately, this provides good first-order correlation between cores from different holes while also avoiding more subjective, and potentially erroneous, interpretations that might arise without applying this restriction first. The mcd scale, once established, provides a basis upon which higher-order depth composite scales can be built.

In essence, the mcd scale overcomes many of the inadequacies of the mbsf depth scale, which is based on drill pipe measurements and is unique to each hole. The mbsf depth scale is based on the length that the drill string is advanced on a core by core basis and is often inaccurate because of ship heave (which is not compensated for in APC coring), tidal variations in sea level, and other sources of error. In contrast, the mcd scale is built by assuming that the uppermost sediment (commonly referred to as the mudline) in the first core from a given hole is the sediment/water interface. This core becomes the "anchor" in the composite depth scale and is typically the only one in which depths are the same on both the mbsf and mcd scales. From this anchor, core logging data are correlated among holes downsection. For each core, a depth offset (a constant) that best aligns the observed lithologic variations to the equivalent cores in adjacent holes is added to the mbsf depth in sequence down the holes. Depth offsets are often chosen to optimize correlation of specific features that define splice levels in cores from adjacent holes.

For Expedition 306, the mcd scale and the splice are based on the stratigraphic correlation of data from the IODP whole-core MSCL, MST, AMST, and long-core magnetometer. For each of these track instruments, data were collected every 2, 2.5, 4, or 5 cm. We used magnetic susceptibility (the data are referred to as MSCL if collected using the MSCL or MS-MST if collected using the MST), gamma ray attenuation (GRA) bulk density, natural gamma radiation (NGR), reflectance (L*, a*, and b*), and the intensity of magnetization following 20 mT AF demagnetization. All of these measurements are described in **"Physical properties"** and **"Paleomagnetism."**

The raw stratigraphic data were imported into Splicer (version 2.2) and culled as necessary to avoid incorporating anomalous data influenced by edge effects at section boundaries. Splicer was used to assess the stratigraphic continuity of the recovered sedimentary sequences at each drill site and to construct the mcd scale and splice.

Because depth intervals within cores are not squeezed or stretched by Splicer, all correlative features cannot be aligned. Stretching or squeezing between cores from different holes may reflect small-scale differences in sedimentation and/or distortion caused by the coring and archiving processes. The tops of APC cores are generally stretched and the bottoms compressed, although this is lithology dependent. In addition, sediment (especially unconsolidated mud, ash, sand, and gravel) occasionally falls from higher levels in the borehole onto the tops of cores as they are recovered, and as a result the top 0–100 cm of many cores are not part of the stratigraphically contiguous section.

Correlations among cores from adjacent holes are evaluated visually and statistically by cross-correlation within a 2 m depth interval, which can be adjusted in size when appropriate. Depth-shifted data are denoted by mcd. A table is presented in each site chapter that summarizes the depth offsets for each core. These tables are necessary for converting mbsf to mcd scales. The mcd for any point within a core equals the mbsf plus the cumulative offset. Correlation at finer resolution is not possible with Splicer because depth adjustments are applied linearly to individual cores; no adjustments, such as squeezing and stretching, are made within cores. Such fine-scale adjustment is possible postcruise (e.g., Hagelberg et al., 1995).

Splicing

Once all cores have been depth-shifted and stratigraphically aligned, a composite section is built by splicing segments together from multiple holes to form a complete record at a site. It is composed of

core sections from adjacent holes so that coring gaps in one hole are filled with core intervals from an adjacent hole. The splice does not contain coring gaps, and an effort has been made to minimize inclusion of disturbed sections. The shipboard splice is ideally suited to guide core sampling for detailed paleoceanographic studies. A table and a figure presented in each site chapter summarize the intervals from each hole used to construct the splice. Additional splices may be constructed postcruise as needed.

The choice of tie points (and hence of a splice) is a somewhat subjective exercise. Our method in the construction of a splice followed three rules. First, where possible we avoided using the top and bottom ~0.5 m of cores, where disturbance resulting from drilling artifacts (even if not apparent in core logging data) was most likely. Second, we attempted to incorporate those portions of the recovered core that were most representative of the overall stratigraphic section of the site. Third, we tried to minimize the number of tie points to simplify sampling.

The length of the spliced section (on the mcd scale) at a given site is typically ~5%–15% greater than the length of the cored section in any one hole as indicated by the mbsf scale. This increase is commonly attributed to sediment expansion resulting from elastic rebound, stretching during the coring process, gas expansion during the core recovery process, and curation practices, in which soupy core material commonly occurring at the top of many cores is curated as part of the core (e.g., Moran, 1997; Acton et al., 2001). In reality, much of the soupy material results from sediment falling into the hole or from sediment being stirred at the bottom of the hole as the BHA is advanced.

Ideally, the base of the mcd scale is the bottom of the deepest core recovered from the deepest hole. In practice, however, the base often occurs where core recovery gaps align across all holes or the data quality does not allow reliable correlations between holes. Cores below this interval cannot be directly tied into the overlying and continuous mcd. However, below the base of the continuous mcd, cores from two or more holes can sometimes be correlated with each other to create a floating splice. In this case an mcd was assigned to the section below the splice by adding the greatest cumulative offset to the first core below the splice and beginning the floating splice from that point in the section.

Corrected meters composite depth

To correct the mcd scale for empirically observed core expansion, a growth factor (GF) is calculated by fitting a line to mbsf versus mcd. By dividing mcd by GF a corrected meters composite depth scale can be evaluated which is a close approximation of the actual drilling depth scale. It should be noted, however, that the actual GF is not linear and varies with lithology.

Magnetic Susceptibility Core Logger

In order to permit rapid stratigraphic correlation for real-time drilling adjustments, the MSCL was used for only the second time during an IODP expedition. The MSCL is a simple track system with two magnetic susceptibility loops separated by 45 cm (see **"Physical properties"**). It was developed to permit rapid measurement of susceptibility on whole-core sections as soon as possible following recovery. The concept was first attempted during ODP Leg 202 using a similar instrument from Oregon State University. During Expedition 303, the current track system was used, but the system did not function properly in dual sensor mode and so only single-sensor data were collected (see **"Physical properties"** in the "Site U1302–U1308 methods" chapter).

Unlike Expedition 303, during Expedition 306 we did not experience any problems with the dual sensors. We were thus able to run the track in dual-sensor mode for all sections measured using a sampling interval of 10 cm for each loop, which results in a 5 cm overall data spacing. Five measurements were made at each interval using SI units and the short (~1 s) measurement setting on the Bartington susceptibility meters. At these settings, we could log a typical 9.5 m long core in ~30 min.

Rare data spikes occurred for reasons yet to be determined, although shielding the cables to the susceptibility meters and keeping cables away from the loops appeared to reduce the frequency of these spikes. These are manifested by single negative values or spikes that differ significantly from real susceptibility values. They were therefore easy to detect and to remove before the data were uploaded into the database. Once in the database, relative offsets between the two meters are mostly removed, providing a consistent data set with higher resolution than could be obtained with a single susceptibility meter in the same amount of time. During Expedition 306, we noted that small systematic differences existed between the two meters even after the offset correction, but these are virtually imperceptible when the data are loaded into Splicer using the five-point smoothing option.

The MSCL susceptibility data are used in Splicer for preliminary stratigraphic correlation with the goal of determining if between-core gaps in one hole correspond with those in a hole that is being cored. If so, drilling adjustments can be made to ensure that co-

eval coring gaps are avoided in subsequent cores. Basically, the stratigraphic correlators are able to guide the drilling in real time to avoid having coeval coring gaps in multiple holes cored at a site, which would result in an incomplete stratigraphic section. This preliminary susceptibility data set is then superceded by the magnetic susceptibility measurements collected on the MST, which is done after the cores have equilibrated to room temperature and generally at higher resolution than on the MSCL. Likewise, the preliminary stratigraphic correlation is superceded by more careful evaluation following the collection of a suite of physical property data and core descriptions.

Depths in splice tables versus Janus depths

The depth of a core interval recorded for a tie point in a splice table is not always the same as the depth for the same core interval returned by most database queries. This is because the tie point depth is based on the liner length, measured when the cores are cut into sections on the catwalk. The cores are analyzed on the MSCL almost immediately after this liner length measurement. At some later time, typically 10 to 36 h after being analyzed by the MST, core sections are split and analyzed further (see **"Core handling and analysis"**). At this time, the section lengths are measured again and are archived as "curated lengths." General database queries return depths based on the curated liner lengths. Because the sections may have expanded during the period between the two measurements or shifted during splitting and handling, the curated length is almost always longer than the initial liner length. Thus, the depths associated with the MST data used to construct the splice table are not identical to the final depths assigned to a given interval by the database. This leads to small differences, usually between 0 and 5 cm, between the mbsf and mcd recorded in a splice table and the depths reported in other places for the same core interval. We have chosen not to change these depths to be compatible with Janus because this would not improve their accuracy. For consistency, we recommend that all postcruise depth models use or build on mcd values provided in the Janus database.

Geochemistry

The shipboard geochemistry program for Expedition 306 included characterization of (1) volatile hydrocarbons, (2) interstitial water, (3) sedimentary inorganic and organic carbon and total nitrogen, and (4) examination of solvent-extractable organic compounds. Volatile hydrocarbon analyses were carried out as part of the routine shipboard safety and pollution prevention requirements.

Sediment gas sampling and analysis

During Expedition 306, the compositions and concentrations of volatile hydrocarbons in the sediments were analyzed once per core using the routine headspace procedure (Pimmel and Claypool, 2001). This procedure involved placing ~5 cm^3 of sediment sample in a 21.5 cm^3 glass serum vial that was sealed with a septum and metal crimp cap immediately after core retrieval on deck. In the shipboard laboratory, the glass vial was heated at 60°C for 30 min. Five cubic centimeters of gas was removed from the headspace in the vial with a glass syringe for analysis by gas chromatography.

Headspace gas samples were analyzed using a Hewlett-Packard 6890 Plus gas chromatograph (GC) equipped with a 2.4 m × 3.2 mm stainless steel column packed with 80/100 mesh HayeSep S and a flame ionization detector (FID). This analytical system measures the concentrations of methane (C_1), ethane (C_2), ethene ($C_{2=}$), propane (C_3), and propene ($C_{3=}$). The sample gas syringe was directly connected to the GC via a 1 cm^3 sample loop. Helium was used as the carrier gas, and the GC oven temperature was held at 90°C. Calibrations were conducted using analyzed gases, and gas concentrations were measured in parts per million by volume.

Interstitial water sampling and chemistry

Interstitial waters were extracted from 5 cm long whole-round sediment sections that were cut and capped immediately after core retrieval on deck. In one hole at each site, samples were taken from each core for the upper 60 mbsf and at intervals of every third core thereafter to a depth of 110 mbsf. In addition to whole-round samples, small plug sediment samples of ~10 cm^3 were taken with a syringe at Site U1313 for shore-based analyses of oxygen isotopes, deuterium, and chloride. These samples were taken at a resolution of two per core for Cores 1 and 2, one per section for Cores 3 through 5, two for Core 6, and one per core for Cores 7, 8, 10, and 11. The small plug samples were taken from the working half at the time of sectioning on deck. This sampling technique was used to obtain high-resolution interstitial water samples while maintaining the integrity of the composite section.

In the shipboard laboratory, whole-round sediment samples were removed from the core liner, and the outside surfaces of the sediment samples were carefully scraped off with spatulas to minimize potential

contamination with drill fluids. Sediment samples were then placed into a Manheim titanium squeezer and squeezed at ambient temperature with a Carver hydraulic press (Manheim and Sayles, 1974). Interstitial water samples discharged from the squeezer were passed through 0.45 µm Whatman polyethersulfone membrane filters, collected in plastic syringes, and stored in plastic sample tubes for shipboard analyses or archived in glass ampoules and/or heat-sealed acid-washed plastic tubes for shore-based analysis. For shipboard inductively coupled plasma–atomic emission spectroscopy (ICP-AES) analysis, 25 µL of concentrated HNO_3 was added to the samples prior storage. The squeezed sediment residues were split in portions of approximately one-quarter and three-quarters. The one-quarter portion was freeze-dried, ground, and used for shipboard organic geochemical analyses (see below). The rest of the portion was stored for shore-based analysis.

Shipboard analyses of whole-round interstitial water samples followed the procedures outlined by Gieskes et al. (1991) and Murray et al. (2000) with modifications as summarized below. Salinity was measured with an Index Instruments digital refractometer. Alkalinity and pH were measured by Gran titration with a Brinkman pH electrode and a Metrohm autotitrator. NH_4^+ concentrations were analyzed by spectrophotometric methods with a Milton Roy spectrophotometer. For the analyses of Mg^{2+}, Ca^{2+}, K^+, Na^+, Mn^{2+}, Fe^{2+}, B, Sr^{2+}, Ba^{2+}, Li^+, and H_4SiO_4 concentrations, a Jobin Yvon JY2000 ICP-AES was used. Concentrations of SO_4^{2-} were determined with a Dionex ion chromatograph. Cl^- was measured by silver nitrate titration method using a Metrohm titrator.

Analytical precision for each of the techniques was monitored through multiple analyses of International Association of Physical Sciences Organization (IAPSO) standard seawater solution or other standard solutions and is reported in Table **T3.**

For calibrations of major elements measured by ICP-AES, IAPSO solutions of Mg^{2+}, Ca^{2+}, K^+, and Na^+ diluted with 18 MS deionized water to 0%, 20%, 40%, 60%, 80%, 100%, 120%, 140%, and 160% were used at the beginning of each batch (i.e., site) run.

Minor elemental analysis by ICP-AES was modified from Murray et al. (2000) as outlined in Shipboard Scientific Party (2003a). Specifically, a "master standard" was prepared by blending certified standard solutions of Mn^{2+}, Fe^{2+}, B, Sr^{2+}, Ba^{2+}, and Li^+ and a silicon reference solution (sodium silicate) in an acidified (1.25% HNO_3, by volume) sodium chloride matrix (17.5 g NaCl/L) diluted with 18 MS deionized water. This solution was diluted to 0%, 3%, 5%, 10%, 30%, 50%, and 100% with a NaCl/HNO_3 matrix (35 g NaCl + 2.5% HNO_3 per 1 L) to generate "working standard" solutions. Calibrations were made for each of the chemical constituents measured on ICP-AES using the working standard solutions diluted with a matrix solution (2.5% HNO_3 + 10 ppm yttrium as an internal standard) prior to each batch (i.e., site) run. Samples were diluted 1:50 for major and 1:10 for minor elements prior to ICP-AES analyses. Chemical data for interstitial water are reported in molar concentration units.

Sedimentary inorganic and organic carbon and nitrogen concentrations

Inorganic carbon concentrations were determined using a Coulometrics 5011 carbon dioxide coulometer equipped with a carbonate analyzer. Two carbonate analyses were performed for each core. Samples of ~10 mg of freeze-dried, ground sediment were reacted with 2N HCl. The liberated CO_2 was backtitrated to a colorimetric end point. Calcium carbonate ($CaCO_3$) content, as weight percent, was calculated from the inorganic carbon (IC) content with the assumption that all inorganic carbon is present as calcium carbonate:

$$CaCO_3\ (wt\%) = IC\ (wt\%) \times 8.33. \quad (1)$$

No corrections were made for other carbonate minerals. The coulometer was calibrated with pure $CaCO_3$ powder during the expedition, and the analytical precision (expressed as 1F standard deviations of means of multiple determinations of a standard) for IC was ±0.45% (for Site U1312).

Total carbon (TC), total nitrogen (TN), and total hydrogen were determined using a Carlo Erba 1500 CHNS analyzer on the same samples used for inorganic carbon concentrations. Aliquots of ~10 mg of freeze-dried, ground sediment and ~10 mg V_2O_5 as co-oxidant were combusted at 1000°C in a stream of oxygen. Nitrogen oxides were reduced to N_2, and the mixture of N_2, CO_2, and H_2O gases was separated by GC and detection performed by a thermal conductivity detector. All measurements were calibrated by comparison to pure sulfanilamide as standard. Analytical precision for TC and TN was 1.99% and 1.07%, respectively (1F standard deviation of means of multiple determinations of sulfanilamide for Sites U1312, U1313, and U1314). Despite low 1F standard deviation for TN, we noticed in sediments from Hole U1314A and partly Hole U1313A that systematic offsets in TN of sample sets run within different batches occurred and initially generated obvious staircase-like downhole profiles. In case of such observations, samples were submitted for rerun. However, shore-based elemental reanalysis of the shipboard samples

will be additionally performed and reported elsewhere.

Contents of total organic carbon (TOC), as weight percent, were calculated as the difference between TC and IC:

$$\text{TOC (wt\%)} = \text{TC (wt\%)} - \text{IC (wt\%)}. \quad (2)$$

As most of the samples had very high $CaCO_3$ contents and very low TOC values (see respective site chapters), the TOC data determined during Expedition 306 should be considered as preliminary, keeping in mind its methodological (i.e., calculated rather then measured) limitation. Indeed, postcruise analysis of shipboard samples from all three sites by means of direct TOC measurement using a LECO CS-125 analyzer (J. Hefter, unpubl. data, 2006) showed no correlation (Fig. **F10**), especially for samples rich in carbonate (>90 wt%, e.g., most of the samples from Hole U1312A).

Solvent-extractable organic compounds

A limited number of sediment samples were analyzed onboard for solvent-extractable organic compounds to determine initial organic matter characteristics for subsequent shore-based analyses (see individual site chapters for numbers and depths). For the shipboard organic geochemistry analyses, freeze-dried splits of one-quarter of whole-round sediment squeeze cakes, used for interstitial water (sampling code IWSG) sampling, were used. To perform the extraction, 10–25 g of sediment was ultrasonically extracted in two 40 mL glass tubes using 20–40 mL CH_2Cl_2 for 15 min. Sediments and solvents were separated in a centrifuge at 2500 rpm for 5 min, and the solvent phase was decanted and collected. The extraction step was repeated by adding 10–20 mL of fresh CH_2Cl_2 to the sediment remnants. The combined total extracts were reduced to near dryness by a gentle stream of N_2. Depending on the amount of TOC and the color of the extracts, total extracts were either directly injected into the GC-mass spectrometer (MS) or further separated by column chromatography. Silica gel (100–200 mesh, dried at 120°C overnight) was placed in a Pasteur pipette plugged with cotton wool and preconditioned by successive elution with 4 mL of CH_2Cl_2 and 4 mL of hexane. Total extracts, redissolved in a small amount (100–200 µL) of hexane, were placed on top and separated into two subfractions by elution with 4 mL of hexane and 4 mL of CH_2Cl_2, respectively. Note that the above analytical procedure will not allow the detection of certain types of compound classes (e.g., fatty acids, alcohols, sterols, etc.) because of the lack of derivatization steps.

The GC-MS system used for compound identification consists of an HP 6890 GC equipped with an HP 7683 automatic liquid sampler and is interfaced via a heated (280°C) transfer line to an HP 5973 mass-selective detector (MSD). Total extracts or subfractions dissolved in a final volume of 100 µL hexane were injected into an electronic pneumatic-controlled split-splitless injector (operated in splitless mode at 300°C; injection volume = 1 µL). Compounds were separated on an HP-5MS capillary column (30 m × 0.25 mm; film thickness = 0.25 µm), using He in constant flow mode (1 mL/min) as carrier gas. The GC temperature program was as follows: 40°C (hold 2 min), heat to 130°C (rate = 20°C/min), heat to 320°C (rate = 4°C/min), and hold 20 min at 320°C. The source temperature of the MSD was set to 230°C and the quadrupole mass analyzer to 150°C. Mass spectra were recorded in full-scan mode from m/z 50 to 600 at a scan rate of 2.7 spectra/s. Compounds were identified by their mass spectral characteristics and GC retention times and by comparison with published mass spectral data or mass spectral databases (NIST, Wiley). Unfortunately, the MS could only be used for Site U1312. Later, the high-voltage supply of the mass analyzer failed and was found not to be repairable for the remaining of the expedition due to the lack of spare electronic parts. As an alternative, we had to use the FID installed on the HP 6890 GC. Identification of *n*-alkanes at the following sites, however, could be established relatively easily by comparison to retention times obtained from a standard mixture containing all homologs from *n*-C_{10} to *n*-C_{36}. The identification of C_{37} and C_{38} alkenones is based on their well-known retention times (e.g., >C_{38} *n*-alkane under the GC conditions used), their specific elution order, and their overall characteristic distribution pattern. Identification of compounds designated as contaminants (mainly plastic-derived, e.g., homologs of phthalate esters) for GC-FID runs is based on previous GC-MS identifications of those compounds in blank and analytical procedure tests and intercomparison of retention times after reruns of the appropriate fractions under GC-FID conditions.

Physical properties

Physical properties were measured on core material recovered during Expedition 306 to

1. Allow real-time stratigraphic correlation and feedback to the drillers;
2. Provide further data for the hole-to-hole core correlation of any given site and for the construction of composite stratigraphic sequences;

3. Detect changes in sediment properties that could be related to lithologic changes, diagenetic features, or consolidation history;
4. Provide the dry density records needed for computing mass accumulation rates;
5. Identify natural and/or coring-induced discontinuities; and
6. Provide data to aid interpretation of seismic reflection and downhole geophysical logs.

Magnetic susceptibility was first measured with the Geotek MSCL on whole-round core sections immediately after recovery. These measurements aided real-time stratigraphic correlation without being limited by the time constraints of MST measurements. After the cores reached room temperature, magnetic susceptibility, GRA bulk density, and NGR were measured on the whole-core MST. Noncontact resistivity was not measured.

Split-core measurements on the working half of the core included V_P with the IODP *P*-wave sensor number 3 (PWS3–measuring perpendicular to the core axis) and moisture and density. A comprehensive description of most of the methodologies and calculations used in the *JOIDES Resolution* physical properties laboratory can be found in Blum (1997).

Magnetic susceptibility MSCL sampling strategy

Rapid stratigraphic correlation of cores from adjacent holes and real-time feedback to drillers for recovering complete stratigraphic sections at all sites was important. An automated dedicated MSCL for rapid measurement of magnetic susceptibility was used to provide a nondestructive proxy of sediment variability to the stratigraphic correlators. Measurements were made as soon as whole-core sections became available. The MSCL system employs a Geotek track system with dual Bartington MS2C meters and two 80 mm inside diameter coils separated by 45 cm. Because of the proximity of the coils to each other, different frequencies were used to reduce interference: 0.621 kHz for the first and 0.513 kHz for the second. Distinct correction factors (1.099 and 0.908, respectively) must be used to synchronize data acquired from the two loops. Measurements were taken every 10 cm. The use of two loops allowed simultaneous interlaced measurements, decreasing the sampling interval to 5 cm. This was fast enough to keep up with core recovery under most circumstances and is significantly faster than the MST logging time. The Geotek uses a core pusher system that measures sections continuously, minimizing edge effects at section breaks. The susceptibility data collected with the MSCL is not appropriate for other uses because cores were measured prior to warming to room temperature and temperature drift corrections were not made.

The MST susceptibility meter (a Bartington MS2C meter with an 80 mm coil diameter driven at 0.565 kHz frequency) was set on SI units, and the output values were stored in the Janus database. The width at half-height of the response function of the susceptibility coil is ~4 cm (Blum, 1997), and the sensing region corresponds to a cored volume of 160. To convert the stored values to SI units of volume susceptibility, values should be multiplied by 10^{-5} and by a correction factor to take into account the volume of material within the response function of the susceptibility coils. For a standard IODP core, this factor is ~6.8×10^{-5} (Thomas et al., 2001), based on laboratory/ship comparisons for Leg 162 sediments. More recent estimates based on Leg 202 sediments suggest a factor of ~6×10^{-5} SI units.

Multisensor track sampling strategy

Magnetic susceptibility, GRA bulk density, and NGR were measured nondestructively on all whole-round core sections with the MST. The noncontact resistivity and compressional wave velocity loggers were not working, and these parameters were not measured. To optimize MST performance, sampling intervals and measurement residence times were the same for all sensors for any one core. Sampling intervals were therefore set at 2.5 or 5 cm, depending on time constraints. These sampling intervals are common denominators of the distances between the sensors installed on the MST (30–50 cm) and allow truly simultaneous measurements and therefore optimal use of total measurement times.

We endeavored to optimize the trade-off between core logging times and depth resolution. Longer analysis times were selected if required to improve measurement precision. These times varied from 3 to 5 s, with most cores measured at 5 s per sample.

The total time availability for MST logging at a site was predicted based on the operational time estimate for the site, subsequent transit time, and any other time available before core was on deck at the subsequent site. Sampling parameters were then optimized to use the total available time (e.g., 2.5 cm and 5 s [~2 h/core]; 5 cm and 5 s [~1.2 h/core]; 5 cm and 3 s [fast logging, ~0.9 h/core]).

Magnetic susceptibility

Magnetic susceptibility is a measure of the degree to which a material can be magnetized by an external magnetic field. It provides information on the magnetic composition of the sediments that often can be related to mineralogical composition (e.g.,

terrigenous versus biogenic materials) and/or diagenetic overprinting. Magnetite and a few other iron oxides with ferromagnetic characteristics have a specific magnetic susceptibility several orders of magnitude higher than clay, which has paramagnetic properties. Carbonate, silica, water, and plastics (core liner) have small and negative values of magnetic susceptibility. Sediments rich in biogenic carbonate and opal therefore have generally low magnetic susceptibility, even negative values, if practically no clay or magnetite is present. In such cases, measured values approach the detection limit of magnetic susceptibility meters.

Magnetic susceptibility was measured with the Bartington Instruments MS2C system on both the MST and the MSCL. The output of the magnetic susceptibility sensors can be set to centimeter-gram-second (cgs) units or SI units.The IODP standard is the SI setting. However, to actually obtain the dimensionless SI volume-specific magnetic susceptibility values, the instrument units stored in the IODP database must be multiplied by a correction factor to compensate for instrument scaling and the geometric ratio between core and loop dimensions, as described above.

A common operational problem with the Bartington meter is that 1 s measurements are rapid but not precise enough for biogenic-rich sediments and the 10 s measurements are much more precise but take a prohibitively long time to measure at the desired sampling interval of 2.5 to 5 cm. The MST program was therefore equipped with the option to average any number of 1 s measurements, and we usually averaged five such measurements.

Gamma ray attenuation bulk density

Bulk density reflects the combined effect of variations in porosity, grain density (dominant mineralogy), and coring disturbance. Porosity is mainly controlled by lithology, texture (e.g., clay, biogenic silica, and carbonate content and grain size and sorting), compaction, and cementation.

The GRA densitometer comprises a 10 mCi ^{137}Cs capsule as the gamma ray source with the principal energy peak at 0.662 MeV and a scintillation detector. The narrow collimated peak is attenuated as it passes through the center of the core. Incident photons are scattered by the electrons of the sediment material by Compton scattering. The attenuation of the incident intensity (I_0) is directly related to the electron density in the sediment core of diameter (D), which can be related to bulk density given the average attenuation coefficient (in micrometers) of the sediment (Harms and Choquette, 1965). Because the attenuation coefficient is similar for most common minerals and aluminum, bulk density is obtained through direct calibration of the densitometer using aluminum rods of different diameters mounted in a core liner that is filled with distilled water. The GRA densitometer has a spatial resolution of <1 cm.

Natural gamma radiation

Terrigenous sediment is often characterized by NGR from K, Th, and U, which are present mostly in clays but can also originate from heavy minerals or lithic grains. Uranium often dominates the NGR in carbonate-rich sediments with little terrigenous input. Uranium concentration is largely controlled by organic matter flux to the seafloor and the existing redox conditions there. It is also mobile and can migrate to certain layers and diagenetic horizons.

The NGR system consists of four shielded scintillation counters with 3 inch × 3 inch doped sodium iodide crystals, arranged at 90° from each other in a plane orthogonal to the core track. The NGR response curve is ~17 cm (full-width half-maximum), an interval that could be considered a reasonable sampling interval. Measurement precision is a direct function (inverse square root) of the total counts (N) accumulated for one measurement, according to Poisson's law of random counting error. N is the product of the intrinsic activity of the material measured and the total measurement time. Therefore, one seeks to maximize the measurement time to improve data quality. Unfortunately, time constraints on core logging during the cruise do not permit long counting times. Furthermore, NGR is measured every 2.5 or 5 cm (same sampling interval as other MST measurements for optimal MST efficiency) and, therefore, only for a relatively short time (typically 5 s). It may be necessary, particularly in low-activity material, to integrate (or smooth) several adjacent measurements to reduce the counting error to an acceptable level. Five-point smoothing is a reasonable data reduction in view of the relatively wide response curve of the sensors. (See Blum, 1997, for more detailed discussions).

P-wave velocity

P-wave velocity in marine sediments varies with the lithology, porosity or bulk density, state of stress such as lithostatic pressure, fabric or degree of fracturing, degree of consolidation and lithification, occurrence and abundance of free gas and gas hydrate, and other properties. *P*-wave velocity was

measured with two systems during Expedition 306, with the MST-mounted *P*-wave logger on whole-round cores (Schultheiss and McPhail, 1989) and with the PWS3 on every section of the split cores. All IODP *P*-wave piezoelectric transducers transmit a 500 kHz compressional wave pulse through the core at a repetition rate of 1 kHz.

Traveltime is determined by the software, which automatically picks the arrival of the first wavelet to a precision of 50 ns. It is difficult for an automated routine to pick the first arrival of a potentially weak signal with significant background noise. The search method applied skips the first positive amplitude and finds the second positive amplitude using a detection threshold limit, typically set to 30% of the maximum amplitude of the signal. Then it finds the preceding zero crossing and subtracts one period to determine the first arrival. To avoid extremely weak signals, minimum signal strength can be set (typically to 0.02 V) and weaker signals are ignored. To avoid cross-talk signals at the beginning of the record from the receiver, a delay (typically set to 0.01 ms) can be set to force the amplitude search to begin in the quiet interval preceding the first arrival. In addition, a trigger (typically 4 V) is selected to initiate the arrival search process.The number of waveforms to be stacked (typically five) can also be set. Linear voltage differential transducers determine length of the travel path.

The *P*-wave velocity systems require two types of calibration, one for the displacement of the transducers and one for the time offset. For the displacement calibration, five acrylic standards of different thickness are measured and the linear voltage-distance relationship determined using least-squares analyses. For the time offset calibration, room-temperature water in a plastic bag is measured multiple times with different transducer displacements. The inverse of the regression slope is equal to the velocity of sound in water, and the intercept represents the delay in the transducers.

Moisture content and density

Samples of 10 cm^3 were taken from the working half sections with a piston minicorer and transferred into previously calibrated 10 mL glass vials. Usually one sample from the top of the first section and the base of the sixth section were taken. Sampling location was coordinated for *P*-wave velocity as well as for subsequent extraction of specimens for carbonate. To minimize the destruction of the available sediment on the specific sampling zones, another 2 cm^3 sample was collected as close as possible to the physical properties sample for carbonate analysis.

Wet and dry weights were determined with twin Scientech 202 electronic balances, which allow for compensation of the ship's motion effect on the balance and give a precision better than 1%.

The samples were dried in a convection oven at a temperature of 105° ± 5°C for a period of 24 h. Dry volume was measured in a He-displacement five-chambered pycnometer with an uncertainty of 0.02 cm^3. This equipment allows the simultaneous analysis of four different samples and a calibration sphere and took ~15–20 min. Three measurements were averaged per sample. The calibration sphere was cycled from cell to cell of the pycnometer during each batch, so that all cells could be checked for accuracy at least once every five runs.

Archive multisensor track sampling strategy

Two instruments were mounted on the AMST, the Minolta spectrophotometer measuring diffuse color reflectance and a point magnetic susceptibility meter, which was not used during this cruise. Color reflectance was measured at 2.0 cm throughout Expedition 306 cores (for color reflectance see **"Lithostratigraphy"**).

Downhole measurements

Downhole logging provides continuous in situ geophysical measurements within a borehole. These measurements are used to assess the physical, chemical, and structural characteristics of formations penetrated by drilling and thus provide a means of reconstructing the stratigraphy, lithology, and mineralogy of a sequence. Well logging is typically undertaken in the deepest hole drilled at any one site. Where core recovery is poor or disturbed, downhole logging data are often the most reliable source of information. Where core recovery is good, core data can be correlated with logging data to refine stratigraphy and unit characterization. Downhole logging operations begin after the hole has been cored and flushed with a viscous drilling fluid. The drilling assembly is then pulled up to ~70 mbsf, and the logging tools are passed through the drill pipe into the open hole. The logging tools are joined together into tool strings so that compatible tools are run together. Each tool string is lowered separately to the base of the hole, and then measurement takes place as the tool string is raised at a constant rate between 275 and 500 m/h (see "Downhole measurements" in the individual site chapters). A wireline heave compensator is used to minimize the effect of the ship's heave on the tool string position in the borehole (Goldberg, 1990). Further information on the procedures and wireline

tools used during Expedition 306 can be found at **iodp.ldeo.columbia.edu/TOOLS_LABS/index.html** and **www.ldeo.columbia.edu/BRG/ODP/LOGGING/index.html.**

Logging tools and tool strings

During Expedition 306, the following logging tool strings were deployed (Fig. **F11;** Table **T4**):

1. The triple combination tool string, which consists of the Hostile Environment Gamma Ray Sonde (HNGS), the Hostile Environment Litho-Density Sonde (HLDS), the Digital Dual Induction Tool model E (DIT-E), and two Lamont-Doherty Earth Observatory–Borehole Research Group (LDEO-BRG) tools, the Multi-Sensor Spectral Gamma Ray Tool (MGT), and the Temperature/Acceleration/Pressure (TAP) tool.
2. The Formation MicroScanner (FMS)-sonic tool string, which consists of the Scintillation Gamma Ray Tool (SGT), the Dipole Sonic Imager (DSI), the General Purpose Inclinometer Tool (GPIT), and the FMS.

Principles and uses of the logging tools

The properties measured by each tool, sampling intervals, and vertical resolutions are summarized in Table **T4.** Explanations of tool name acronyms and their measurement units are summarized in Table **T5.** More detailed descriptions of individual logging tools and their geological applications can be found in Ellis (1987), Goldberg (1997), Rider (1996), Schlumberger (1989, 1994), Serra (1984, 1986, 1989), and the LDEO-BRG Wireline Logging Services Guide (1994).

Natural radioactivity

Three wireline spectral gamma ray tools were used during Expedition 306 to measure and classify natural radioactivity in the formation: the HNGS, the SGT, and the LDEO-BRG MGT. The HNGS measures the natural gamma radiation from isotopes of K, Th, and U and uses a five-window spectroscopic analysis to determine concentrations of radioactive ^{40}K (in weight percent), ^{232}Th (in parts per million), and ^{238}U (in parts per million). The HNGS uses two bismuth germanate scintillation detectors for gamma ray detection with full spectral processing. The spectral analysis filters out gamma ray energies below 500 keV, eliminating sensitivity to bentonite or potassium chloride (KCl) in the drilling mud and improving measurement accuracy. The HNGS also provides a measure of the total standard gamma ray emission and uranium-free or computed gamma ray emission that are measured in gAPI. The HNGS response is influenced by the borehole diameter and the weight and concentration of bentonite or KCl present in the drilling mud. KCl may be added to the drilling mud to prevent freshwater clays from swelling and forming obstructions. All of these effects are corrected during processing of HNGS data at LDEO-BRG.

The SGT uses a sodium iodide scintillation detector to measure the total natural gamma ray emission, combining the spectral contributions of ^{40}K, ^{238}U, and ^{232}Th concentrations in the formation. The SGT is not a spectral tool but provides high-resolution total gamma ray data for depth correlation between logging strings. It is included in the FMS-sonic tool string to provide a reference log to correlate and depth between different logging runs. In the FMS-sonic tool string, the SGT is placed between the two tools, providing correlation data to a deeper level in the hole.

The MGT was developed by LDEO-BRG to improve the vertical resolution of natural gamma ray logs by using an array of four short detector modules with 60 cm spacing. Each module comprises a small 2 inch × 4 inch NaI detector, a programmable 256-channel amplitude analyzer, and a ^{241}Am calibration source. The spectral data are subsequently recalculated to determine the concentration of K, Th, and U radioisotopes or their equivalents. The spectral data from individual modules are sampled four times per second and stacked in real time based on the logging speed. This approach increases vertical resolution by a factor of two to three over conventional tools while preserving comparable counting efficiency and spectral resolution. The radius of investigation depends on several factors: hole size, mud density, formation bulk density (denser formations display a slightly lower radioactivity), and the energy of the gamma rays (a higher-energy gamma ray can reach the detector from deeper in the formation). The MGT also includes an accelerometer channel to improve data stacking by the precise measurement of logging speed. Postcruise corrections for borehole size and tool sticking, based respectively on the caliper and acceleration data, are possible.

Density

Formation density was determined with the HLDS. The tool contains a radioactive cesium (^{137}Cs) gamma ray source (622 keV) and far and near gamma ray detectors mounted on a shielded skid that is pressed against the borehole wall by a hydraulically activated eccentralizing arm. Gamma rays emitted by the source experience both Compton scattering and photoelectric absorption. Compton scattering involves the ricochet of gamma rays off electrons in the formation via elastic collision, transferring en-

ergy to the electron in the process. The number of scattered gamma rays that reach the detectors is directly related to the number of electrons in the formation, which is related to bulk density. Porosity may also be derived from this bulk density if the matrix density is known.

The HLDS also measures the photoelectric effect factor (PEF) caused by absorption of low-energy gamma radiation. Photoelectric absorption occurs when gamma radiation reaches <150 keV after being repeatedly scattered by electrons in the formation. As the PEF depends on the atomic number of the elements in the formation, it is essentially independent of porosity. Thus, the PEF varies according to the chemical composition of the formation. PEF values can be used in combination with HNGS curves to identify different types of clay minerals. Coupling between the tool and borehole wall is essential for good HLDS logs. Poor contact results in underestimation of density values. Both density correction and caliper measurement of the hole are used to check the contact quality.

Porosity

Formation porosity was measured with the APS. The sonde incorporates a minitron neutron generator that produces fast neutrons (14.4 MeV) and five neutron detectors (four epithermal and one thermal) positioned at differing intervals from the minitron. The measurement principle involves counting neutrons that arrive at the detectors after being slowed by neutron absorbers surrounding the tool. The highest energy loss occurs when neutrons collide with hydrogen nuclei, which have practically the same mass as the neutron (the neutrons simply bounce off heavier elements without losing much energy). If hydrogen concentration is low, as in low-porosity formations, neutrons can travel farther before being captured, and the count rates increase at the detector. The opposite effect occurs when the water content is high. However, because hydrogen bound in minerals such as clays or in hydrocarbons also contributes to the measurement, the raw porosity value is often an overestimate. Upon reaching thermal energies (0.025 eV), the neutrons are captured by the nuclei of Cl, B, Cd, and other rare earth and trace elements with large capture cross sections, resulting in a gamma ray emission. This neutron capture cross section (3_f) is also measured by the tool.

Electrical resistivity

The DIT-E was used to measure electrical resistivity. The DIT-E provides three measures of electrical resistivity, each with a different depth of penetration. The two induction devices (deep and medium depths of penetration) transmit high-frequency alternating currents through transmitter coils, creating magnetic fields that induce secondary currents in the formation. These currents produce a new inductive signal, proportional to the conductivity of the formation, which is measured by the receiving coils. The measured conductivities are then converted to resistivity (measured in ohm-meters). For the shallow-penetration resistivity, the current necessary to maintain a constant voltage drop across a fixed interval is measured; it is a direct measurement of resistivity. Sand grains and hydrocarbons are electrical insulators, whereas ionic solutions and clays are more conductive. Electrical resistivity can therefore be used to evaluate porosity (by Archie's law) if fluid salinity is known.

Temperature, acceleration, and pressure

Downhole temperature, acceleration, and pressure were measured with the LDEO-BRG high-resolution TAP tool run in memory mode. The tool uses fast- and slow-response thermistors to detect borehole fluid temperature at two different rates. The fast-response thermistor detects small, abrupt changes in temperature, whereas the slow-response thermistor more accurately estimates temperature gradients and thermal regimes. A pressure transducer is used to activate the tool at a specified depth, typically 200 m above seafloor. A three-axis accelerometer measures tool movement downhole, providing data for analyzing the effects of heave on a deployed tool string. The acceleration log can aid in deconvolving heave effects postcruise. The elapsed time between the end of drilling and the logging operation is generally not sufficient to allow the borehole to reach thermal equilibrium following circulation of the drilling fluid. Nevertheless, it is possible to identify abrupt temperature changes that may represent localized fluid flow into the borehole, indicative of fluid pathways and fracturing and/or breaks in the temperature gradient that may correspond to contrasts in permeability at lithologic boundaries.

Acoustic velocity

The DSI measures the transit times between sonic transmitters and an array of eight receivers. It averages replicate measurements, thus providing a direct measurement of sound velocity through sediments that is relatively free from the effects of formation damage and borehole enlargement (Schlumberger, 1989). The tool contains the monopole transmitters found on most sonic tools but also has two cross-dipole transmitters, providing shear wave velocity measurement in addition to the compressional wave velocity, even in the slow formations typically encountered during IODP expeditions.

Formation MicroScanner

The FMS provides high-resolution electrical resistivity–derived images of the borehole (~30% of a 25 cm diameter borehole on each pass). The vertical resolution of FMS images is ~5 mm, allowing features such as clasts, thin beds, and bioturbation to be imaged. The resistivity measurements are converted to color or grayscale images for display. The tool uses four orthogonal imaging pads, each containing 16 button electrodes that are pressed against the borehole wall during the recording. A focused current is emitted from the button electrodes into the formation, with a return electrode near the top of the tool. The intensity of current passing through the button electrodes is measured and converted to an image. With the FMS tool, features such as bedding, fracturing, slump folding, and bioturbation can be resolved, and spatially oriented images allow fabric analysis and bed orientations to be measured (Luthi, 1990; Lovell et al., 1998; Salimullah and Stow, 1992). The maximum extension of the caliper arms is 15 inches, so in holes or parts of holes where the diameter is larger the pad contact will be inconsistent and the FMS images may appear out of focus and too conductive. Irregular borehole walls will also adversely affect the image quality if it leads to poor pad-wall contact.

In site chapters in this volume, local contrasts in FMS images were improved by applying dynamic and static normalizations to the FMS data. A linear gain is applied, which keeps a constant mean and standard deviation within a sliding window of ~1 m or the entire logged interval, respectively. FMS images are oriented to magnetic north using the GPIT. This method allows the dip and strike of geological features intersecting the hole to be measured from processed FMS images.

Accelerometry and magnetic field measurement

Three-component acceleration and magnetic field measurements were made with the GPIT. The primary purpose of this tool, which incorporates a three-component accelerometer and a three-component magnetometer, is to determine the acceleration and orientation of the FMS-sonic tool string during logging. This provides a means of correcting the FMS images for irregular tool motion, allowing the true dip and direction (azimuth) of structures to be determined.

Wireline logging data quality

Logging data quality may be seriously degraded by changes in the hole diameter and in sections where the borehole diameter greatly decreases or is washed out. Deep-investigation measurements such as resistivity and sonic velocity are least sensitive to borehole conditions. Nuclear measurements (density and neutron porosity) are more sensitive because of their shallower depth of investigation and the effect of drilling fluid volume on neutron and gamma ray attenuation. Corrections can be applied to the original data to reduce these effects. HNGS and SGT data provide a depth correlation between logging runs. Logs from different tool strings may, however, still have depth mismatches caused by either cable stretch or ship heave during recording.

Logging depth scales

The depth of the wireline-logged measurement is determined from the length of the logging cable paid out at the winch on the ship. The seafloor is identified on the natural gamma log by the abrupt reduction in gamma ray count at the water/sediment boundary (mudline). Discrepancies between the drillers depth and the wireline logging depth occur because of incomplete heave compensation, tidal changes, and cable stretch (~1 m/km) in the case of logging depth. The small differences between drill pipe depth and logging depth, and the even more significant discrepancy between IODP curation depth and logging depth, should be taken into account when using the logs for correlation between core and logging data. Core measurements, such as susceptibility and density, can be correlated with the equivalent downhole logs using the Sagan program, which allows linear shifting of the core depths onto the logging depth scale.

Logging data flow and processing

After logging was completed in each hole, data were transferred to the shipboard downhole measurements laboratory for preliminary processing and interpretation. FMS image data were interpreted using Schlumberger's Geoframe (version 4.0.4.1) software package. Logging data were also transmitted onshore for processing soon after each hole was logged. Onshore data processing consisted of (1) depth-shifting all logs relative to a common datum (i.e., in mbsf), (2) corrections specific to individual tools, and (3) quality control and rejection of unrealistic or spurious values. Once processed onshore, the data were transmitted back to the ship, providing final processed logging results during the expedition. Processed data were then replotted onboard (see "Downhole measurements" section in each site chapter). Postcruise-processed data in ASCII format are available directly from the IODP–USIO, Science Services, LDEO Internet World Wide Web site at **iodp.ldeo.columbia.edu/DATA/IODP/index.html.**

References

Acton, G.D., Borton, C.J., and the Leg 178 Shipboard Scientific Party, 2001. Palmer Deep composite depth scales for Leg 178 Sites 1098 and 1099. *In* Barker, P.F., Camerlenghi, A., Acton, G.D., and Ramsay, A.T.S. (Eds.), *Proc. ODP, Sci. Results,* 178, 1–35 [Online]. Available from World Wide Web **http://www-odp.tamu.edu/publications/178_SR/VOLUME/CHAPTERS/SR178_05.PDF.**

Aguirre, E., and Pasini, G., 1985. The Pliocene–Pleistocene boundary. *Episodes,* 8:11–120.

Akiba, F., and Yanagisawa, Y., 1986. Taxonomy, morphology and phylogeny of the Neogene diatom zonal marker species in the middle-to-high latitudes of the North Pacific. *In* Kagami, H., Karig, D.E., Coulbourn, W.T., et al., *Init. Repts. DSDP,* 87: Washington (U.S. Govt. Printing Office), 483–554.

Altenbach, A.V., Lutze, G.F., Schiebel, R., and Schoenfeld, J., 2003. Impact of interrelated and independent ecological controls on benthic foraminifera: an example from the Gulf of Guinea. *Paleogeogr., Paleoclimatol., Paleoecol.,*197:213–238. **doi:10.1016/S0031-0182(03)00463-2**

Backman, J., and Raffi, I., 1997. Calibration of Miocene nannofossil events to orbitally tuned cyclostratigraphies from Ceara Rise. *In* Shackleton, N.J., Curry, W.B., Richter, C., and Bralower, T.J. (Eds.), *Proc. ODP, Sci. Results,* 154: College Station, TX (Ocean Drilling Program), 83–99. [**PDF**]

Baldauf, J.G., 1985. Cenozoic diatom biostratigraphy and paleoceanography of the Rockall Plateau region, North Atlantic, Deep Sea Drilling Project Leg 81. *In* Roberts, D.G., Schnitker, D., et al., *Init. Repts. DSDP,* 81: Washington (U.S. Govt. Printing Office), 439–478.

Baldauf, J.G., 1987. Diatom biostratigraphy of the middle- and high-latitude North Atlantic Ocean, Deep Sea Drilling Project Leg 94. *In* Ruddiman, W.F., Kidd, R.B., Thomas, E., et al., *Init. Repts. DSDP,* 94 (Pt. 2): Washington (U.S. Govt. Printing Office), 729–762.

Balsam, W.L., and Damuth, J.E., 2000. Further investigations of shipboard vs. shore-based spectral data: implications for interpreting Leg 164 sediment composition. *In* Paull, C.K., Matsumoto, R., Wallace, P., and Dillon, W.P. (Eds.), *Proc. ODP, Sci. Results,* 164: College Station, TX (Ocean Drilling Program), 313–324. [**HTML**]

Balsam, W.L., Deaton, B.C., and Damuth, J.E., 1998. The effects of water content on diffuse reflectance spectrophotometry studies of deep-sea sediment cores. *Mar. Geol.,* 149:177–189. **doi:10.1016/S0025-3227(98)00033-4**

Balsam, W.L., Damuth, J.E., and Schneider, R.R., 1997. Comparison of shipboard vs. shore-based spectral data from Amazon-Fan Cores: implications for interpreting sediment composition. *In* Flood, R.D., Piper, D.J.W., Klaus, A., and Peterson, L.C. (Eds.), *Proc. ODP, Sci. Results,* 155: College Station, TX (Ocean Drilling Program), 193–215. [**PDF**]

Barron, J.A., 1985. Late Eocene to Holocene diatom biostratigraphy of the equatorial Pacific Ocean, Deep Sea Drilling Project Leg 85. *In* Mayer, L., Theyer, F., Thomas, E., et al., *Init. Repts. DSDP,* 85: Washington (U.S. Govt. Printing Office), 413–456.

Blum, P., 1997. Physical properties handbook: a guide to the shipboard measurement of physical properties of deep-sea cores. *ODP Tech. Note,* 26 [Online]. Available from World Wide Web: **http://www-odp.tamu.edu/publications/tnotes/tn26/INDEX.HTM.**

Burckle, L.H., 1972. Late Cenozoic planktonic diatom zones from the eastern equatorial Pacific. *In* Simonsen, R. (Ed.), *First Symposium on Recent and Fossil Marine Diatoms.* Nova Hedwegia Beih., 39:217–246.

Burckle, L.H., 1977. Neogene diatom correlations in the Circum-Pacific. *Proc. 1st Int. Congress Pacific Neogene Stratigraphy,* 36–39.

Cande, S.C., and Kent, D.V., 1995. Revised calibration of the geomagnetic polarity timescale for the Late Cretaceous and Cenozoic. *J. Geophys. Res.,* 100:6093–6095. **doi:10.1029/94JB03098**

Channell, J.E.T., Labs, J., and Raymo, M.E., 2003. The Reunion Subchronzone at ODP Site 981 (Feni Drift, North Atlantic). *Earth Planet. Sci. Lett.,* 215:1–12. **doi:10.1016/S0012-821X(03)00435-7**

Channell, J.E.T., Mazaud, A., Sullivan, P., Turner, S., and Raymo, M.E., 2002. Geomagnetic excursions and paleointensities in the Matuyama Chron at ODP Sites 983 and 984 (Iceland Basin). *J. Geophys. Res.,* 107. **doi:10.1029/2001JB000491**

Curry, W.B., Shackleton, N.J., Richter, C., et al., 1995. *Proc. ODP, Init. Repts.,* 154: College Station, TX (Ocean Drilling Program).

de Kaenel, E., Siesser, W.G., and Murat, A., 1999. Pleistocene calcareous nannofossil biostratigraphy and the western Mediterranean sapropels, Sites 974 to 977 and 979. *In* Zahn, R., Comas, M.C., and Klaus, A. (Eds.), *Proc. ODP, Sci. Results,* 161: College Station, TX (Ocean Drilling Program), 159–183. [**HTML**]

Droser, M.L., and Bottjer, D.J., 1986. A semiquantitative field classification of ichnofabric. *J. Sediment. Petrol.,* 56:558–559.

Ellis, D.V., 1987. *Well Logging for Earth Scientists:* New York (Elsevier).

Gersonde, R., Hodell, D.A., Blum, P., et al., 1999. *Proc. ODP, Init. Repts.,* 177 [CD-ROM]. Available from: Ocean Drilling Program, Texas A&M University, College Station, TX 77845-9547, U.S.A. [**HTML**]

Gieskes, J.M., Gamo, T., and Brumsack, H., 1991. Chemical methods for interstitial water analysis aboard *JOIDES Resolution. ODP Tech. Note,* 15 [Online]. Available from World Wide Web: **http://www-odp.tamu.edu/publications/tnotes/tn15/f_chem1.htm.**

Goldberg, D., 1990. Test performance of the Ocean Drilling Program wireline heave motion compensator. *Sci. Drill.,* 1:206–209.

Goldberg, D., 1997. The role of downhole measurements in marine geology and geophysics. *Rev. Geophys.,* 35:315–342. **doi:10.1029/97RG00221**

Goll, R.M., and Bjørklund, K.R., 1989. A new radiolarian biostratigraphy for the Neogene of the Norwegian Sea: ODP Leg 104. *In* Eldholm, O., Thiede, J., Taylor, E., et

al., *Proc. ODP, Sci. Results,* 104: College Station, TX (Ocean Drilling Program), 697–737. [PDF]

Hagelberg, T., Shackleton, N., Pisias, N., and Shipboard Scientific Party, 1992. Development of composite depth sections for Sites 844 through 854. *In* Mayer, L., Pisias, N., Janecek, T., et al., *Proc. ODP, Init. Repts.,* 138 (Pt. 1): College Station, TX (Ocean Drilling Program), 79–85.

Hagelberg, T.K., Pisias, N.G., Shackleton, N.J., Mix, A.C., and Harris, S., 1995. Refinement of a high-resolution, continuous sedimentary section for studying equatorial Pacific Ocean paleoceanography, Leg 138. *In* Pisias, N.G., Mayer, L.A., Janecek, T.R., Palmer-Julson, A., and van Andel, T.H. (Eds.), *Proc. ODP, Sci Results,* 138: College Station, TX (Ocean Drilling Program), 31–46.

Harms, J.C., and Choquette, P.W., 1965. Geologic evaluation of a gamma-ray porosity device. *Trans. SPWLA 6th Ann. Logging Symp.:* Dallas, C1–C37.

Haslett, S.K., 1994. Plio–Pleistocene radiolarian biostratigraphy and paleoceanography of the mid-latitude North Atlantic (DSDP Site 609). *Geol. Mag.*, 131:57–66.

Haslett, S.K., 2004. Late Neogene–Quaternary radiolarian biostratigraphy: a brief review. *J. Micropaleontol.*, 23:39–47.

Hayward, B.W., 2001. Global deep-sea extinctions during the Pleistocene ice-ages. *Geology,* 29:599–602. doi:10.1130/0091-7613(2001)029<0599:GDSEDT>2.0.CO;2

Hilgen, F.J., Krijgsman, W., Langereis, C.G., Lourens, L.J., Santarelli, A., and Zachariasse, W.J., 1995. Extending the astronomical (polarity) time scale into the Miocene. *Earth Planet. Sci. Lett.,* 136:495–510. doi:10.1016/0012-821X(95)00207-S

Hilgen, F.J., Krijgsman, W., Raffi, I., Turco, E., and Zachariasse, W.J., 2000. Integrated stratigraphy and astronomical calibration of the Serravallian/Tortonian boundary section at Monte Gibliscemi (Sicily, Italy). *Mar. Micropaleontol.,* 38:181–211. doi:10.1016/S0377-8398(00)00008-6

Hodell, D.A., Curtis, J.H., Sierro, F.J., and Raymo, M.E., 2001. Correlation of late Miocene to early Pliocene sequences between the Mediterranean and North Atlantic. *Paleoceanogr.*, 16:164–178. doi:10.1029/1999PA000487

Jansen, E., Raymo, M.E., Blum, P., et al., 1996. *Proc. ODP, Init. Repts.,* 162: College Station, TX (Ocean Drilling Program).

Jorissen, F.J., de Stigter, H.C., and Widmark, J.G.V., 1995. A conceptual model explaining benthic foraminiferal microhabitats. *Mar. Micropaleontol.,* 26:3–15. doi:10.1016/0377-8398(95)00047-X

Kennett, J.P., and Srinivasan, M.S., 1983. *Neogene Planktonic Foraminifera: A Phylogenetic Atlas:* Stroudsburg, PA (Hutchinson Ross).

Koç, N., Hodell, D.A., Kleiven, H., and Labeyrie, L., 1999. High–resolution Pleistocene diatom biostratigraphy of Site 983 and correlations with isotope stratigraphy. *In* Raymo, M.E., Jansen, E., Blum, P., and Herbert, T.D. (Eds.), 1999. *Proc. ODP, Sci. Results,* 162: College Station, TX (Ocean Drilling Program), 51–62. [HTML]

Koizumi, I., 1973. The late Cenozoic diatoms of Sites 183–193, Leg 19 Deep Sea Drilling Project. *In* Creager, J.S., Scholl, D.W., et al., *Init. Repts. DSDP,* 19: Washington (U.S. Govt. Printing Office), 805–855.

Krijgsman, W., Hilgen, F.J., Langereis, C.G., Santaralli, A., and Zachariasse, W.J., 1995. Late Miocene magnetostratigraphy, biostratigraphy and cyclostratigraphy in the Mediterranean. *Earth Planet. Sci. Lett.*, 136:475–494. doi:10.1016/0012-821X(95)00206-R

Lamont-Doherty Earth Observatory-Borehole Research Group, 1994. *Wireline Logging Services Guide* [Online]. Available from World Wide Web: http://www.ldeo.columbia.edu/BRG/ODP/LOGGING/.

Lazarus, D., and Pallant, A., 1989. Oligocene and Neogene radiolarians from the Labrador Sea, ODP Leg 105. *In* Srivastava, S.P., Arthur, M.A., Clement, B., et al., *Proc. ODP, Sci. Results,* 105: College Station, TX (Ocean Drilling Program), 349–380.

Loeblich, A.R., and Tappan, H., 1988. *Foraminiferal Genera and Their Classification* (Vol. 1 and 2): New York (Van Nostrand Reinhold Co.).

Lourens, L.J., Antonarakou, A., Hilgen, F.J., Van Hoof, A.A.M., Vergnaud-Grazzini, C., and Zachariasse, W.J., 1996. Evaluation of the Plio–Pleistocene astronomical timescale. *Paleoceanography,* 11:391–413.

Lovell, M.A., Harvey, P.K., Brewer, T.S., Williams, C., Jackson, P.D., and Williamson, G., 1998. Application of FMS images in the Ocean Drilling Program: an overview. *In* Cramp, A., MacLeod, C.J., Lee, S.V., and Jones, E.J.W. (Eds.), *Geological Evolution of Ocean Basins: Results from the Ocean Drilling Program*. Geol. Soc. Spec. Publ., 131:287–303.

Luthi, S.M., 1990. Sedimentary structures of clastic rocks identified from electrical borehole images. *In* Hurst, A., Lovell, M.A., and Morton, A.C. (Eds.), *Geological Applications of Wireline Logs*. Spec. Publ.—Geol. Soc. London, 48:3–10.

Lyle, M., Koizumi, I., Richter, C., et al., 1997. *Proc. ODP, Init. Repts.,* 167: College Station, TX (Ocean Drilling Program). [PDF]

Manheim, F.T., and Sayles, F.L., 1974. Composition and origin of interstitial waters of marine sediments, based on deep sea drill cores. *In* Goldberg, E.D. (Ed.), *The Sea* (Vol. 5): *Marine Chemistry: The Sedimentary Cycle:* New York (Wiley), 527–568.

Martini, E., 1971. Standard Tertiary and Quaternary calcareous nannoplankton zonation. *In* Farinacci, A. (Ed.), *Proc. 2nd Int. Conf. Planktonic Microfossils Roma:* Rome (Ed. Tecnosci.), 2:739–785.

Mazzullo, J.M., Meyer, A., and Kidd, R.B., 1988. New sediment classification scheme for the Ocean Drilling Program. *In* Mazzullo, J.M., and Graham, A.G. (Eds.), Handbook for shipboard sedimentologists. *ODP Tech. Note,* 8:45–67.

Mix, A.C., Tiedemann, R., Blum, P., et al., 2003. *Proc. ODP, Init. Repts.,* 202 [CD-ROM]. Available from: Ocean Drilling Program, Texas A&M University, College Station TX 77845-9547, USA. [HTML]

Moran, K., 1997. Elastic property corrections applied to Leg 154 sediment, Ceara Rise. *In* Shackleton, N.J., Curry,

W.B., Richter, C., and Bralower, T.J. (Eds.), *Proc. ODP, Sci. Results,* 154: College Station, TX (Ocean Drilling Program), 151–155. [PDF]

Munsell Color Company, 1992. *Munsell Soil Color Charts,* Newburgh, NY (MacBeth Division of Kollmorgen Instruments Corp.).

Murray, R.W., Miller, D.J., and Kryc, K.A., 2000. Analysis of major and trace elements in rocks, sediments, and interstitial waters by inductively coupled plasma–atomic emission spectrometry (ICP-AES). *ODP Tech. Note,* 29 [Online]. Available from World Wide Web: **http://www-odp.tamu.edu/publications/tnotes/tn29/INDEX.HTM.**

Pimmel, A., and Claypool, G., 2001. Introduction to shipboard organic geochemistry on the *JOIDES Resolution. ODP Tech. Note,* 30 [Online]. Available from World Wide Web: **http://www-odp.tamu.edu/publications/tnotes/tn30/INDEX.HTM.**

Raffi, I., and Flores, J.-A., 1995. Pleistocene through Miocene calcareous nannofossils from eastern equatorial Pacific Ocean. *In* Pisias, N.G., Mayer, L.A., Janecek, T.R., Palmer-Julson, A., and van Andel, T.H. (Eds.), *Proc. ODP, Sci. Results,* 138: College Station, TX (Ocean Drilling Program), 233–286.

Rider, M.H., 1996. *The Geological Interpretation of Well Logs* (2nd ed.): Caithness (Whittles Publishing).

Ruddiman, W.F., Cameron, D., and Clement, B.M., 1987. Sediment disturbance and correlation of offset holes drilled with the hydraulic piston corer: Leg 94. *In* Ruddiman, W.F., Kidd, R.B., Thomas, E., et al., *Init. Repts. DSDP,* 94 (Pt. 2): Washington (U.S. Govt. Printing Office), 615–634.

Salimullah, A.R.M., and Stow, D.A.V., 1992. Application of FMS images in poorly recovered coring intervals: examples from ODP Leg 129. *In* Hurst, A., Griffiths, C.M., and Worthington, P.F. (Eds.), *Geological Application of Wireline Logs II.* Geol. Soc. Spec. Publ., 65:71–86.

Sato, T., Kameo, K., and Mita, I., 1999. Validity of the latest Cenozoic calcareous nannofossil datums and its application to the tephrochronology. *Earth Sci.,* 53:265–274.

Schlumberger, 1989. *Log Interpretation Principles/Applications:* Houston (Schlumberger Educ. Services), SMP–7017.

Schlumberger, 1994. *Log Interpretation Charts:* Sugarland, TX (Schlumberger Wireline and Testing), SMP-7006.

Schrader, H.J., and Gersonde, R., 1978. Diatoms and silicoflagellates. *In* Zachariasse, W.J., et al. (Eds.), *Micropaleontological Counting Methods and Techniques: An Exercise of an Eight Metres Section of the Lower Pliocene of Cap Rossello, Sicily.* Utrecht Micropaleontol. Bull., 17:129–176.

Schultheiss, P.J., and McPhail, S.D., 1989. An automated *P*-wave logger for recording fine-scale compressional wave velocity structures in sediments. *In* Ruddiman, W., Sarnthein, M., et al., *Proc. ODP, Sci. Results,* 108: College Station, TX (Ocean Drilling Program), 407–413. [PDF]

Serra, O., 1984. *Fundamentals of Well-Log Interpretation* (Vol. 1): *The Acquisition of Logging Data:* Dev. Pet. Sci., 15A: Amsterdam (Elsevier).

Serra, O., 1986. *Fundamentals of Well-Log Interpretation* (Vol. 2): *The Interpretation of Logging Data.* Dev. Pet. Sci., 15B: Amsterdam (Elsevier).

Serra, O., 1989. *Formation MicroScanner Image Interpretation:* Houston (Schlumberger Educ. Services), SMP-7028.

Shackleton, N.J., Crowhurst, S., Hagelberg, T., Pisias, N.G., and Schneider, D.A., 1995. A new late Neogene time scale: application to Leg 138 sites. *In* Pisias, N.G., Mayer, L.A., Janecek, T.R., Palmer-Julson, A., and van Andel, T.H. (Eds.), *Proc. ODP, Sci. Results,* 138: College Station, TX (Ocean Drilling Program), 73–101.

Shipboard Scientific Party, 2000. Explanatory notes. *In* Sacks, I.S., Suyehiro, K., Acton, G.D., et al., *Proc. ODP, Init. Repts.*, 186, 1–51 [CD-ROM]. Available from: Ocean Drilling Program, Texas A&M University, College Station TX 77845-9547, USA. [HTML]

Shipboard Scientific Party, 2003a. Explanatory notes. *In* Mix, A.C., Tiedemann, R., Blum, P., et al., *Proc. ODP, Init. Repts.,* 202, 1–76 [CD_ROM]. Available from: Ocean Drilling Program, Texas A&M University, College Station TX 77845-9547, USA. [HTML]

Shipboard Scientific Party, 2003b. Explanatory notes. *In* Wilson, D.S., Teagle, D.A.H., Acton, G.D., *Proc. ODP, Init. Repts.,* 206, 1–94 [CD-ROM]. Available from: Ocean Drilling Program, Texas A&M University, College Station TX 77845-9547, USA. [HTML]

Sierro, F.J., Hilgen, F.J., Krijgsman, W., and Flores, J.A., 2001. The Abad composite (SE Spain): a Messinian reference section for the Mediterranean and the APTS. *Paleogeogr., Paleoclimatol., Paleoecol.,* 168:141–169. **doi:10.1016/S0031-0182(00)00253-4**

Sierro, F.J., Flores, J.A., Civis, J., González-Delgado, J.A., and Frances, G., 1993. Late Miocene globorotaliid event-stratigraphy and biogeography in the NE-Atlantic and Mediterranean. *Mar. Micropaleontol.,* 21:143–168. **doi:10.1016/0377-8398(93)90013-N**

Spezzaferri, S., 1998. Planktonic foraminifer biostratigraphy and paleoenvironmental implications of Leg 152 sites (East Greenland Margin). *In* Saunders, A.D., Larsen, H.C., and Wise, S.W., Jr. (Eds.), *Proc. ODP, Sci. Results,* 152: College Station, TX (Ocean Drilling Program), 161–189. [PDF]

Takayama, T., and Sato, T., 1987. Coccolith biostratigraphy of the North Atlantic Ocean, Deep Sea Drilling Project Leg 94. *In* Ruddiman, W.F., Kidd, R.B., Thomas, E., et al., *Init. Repts. DSDP,* 94 (Pt. 2): Washington (U.S. Govt. Printing Office), 651–702.

Takayama, T., and Sato, T., 1993–1995. Coccolith biostratigraphy of the Pliocene/Pleistocene boundary stratotype. *Ann. Geol. Pays Hell.,* 36:143–150.

Thomas, R.G., Guyodo, Y., and Channell, J.E.T., 2003. U channel track for susceptibility measurements. *Geochem., Geophys., Geosyst.,* 4(6). **doi:10.1029/2002GC000454**

Wang, P., Prell, W.L., Blum, P., et al., 2000. *Proc. ODP, Init. Repts.,* 184 [CD-ROM]. Available from: Ocean Drilling Program, Texas A&M University, College Station TX 77845-9547, USA. [HTML]

Weaver, P.P.E., and Clement, B.M., 1987. Magnetobiostratigraphy of planktonic foraminiferal datums, DSDP

Leg 94, North Atlantic. *In* Ruddiman, W.F., Kidd, R.B., Thomas, E., et al., *Init. Repts. DSDP,* 94: Washington (U.S. Govt. Printing Office), 815–829.

Wentworth, C.K., 1922. A scale of grade and class terms of clastic sediments. *J. Geol.,* 30:377–392.

Westberg-Smith, M.J., and Riedel, W.R., 1984. Radiolarians from the western margin of the Rockall Plateau: Deep Sea Drilling Project Leg 81. *In* Roberts, D.G., Schnitker, D., et al., *Init. Repts. DSDP,* 81: Washington (U.S. Govt. Printing Office), 479–501.

Zachos, J.C., Kroon, D., Blum, P., et al., 2004. *Proc. ODP, Init. Repts.,* 208 [CD-ROM]. Available from: Ocean Drilling Program, Texas A&M University, College Station TX 77845-9547, USA. [**HTML**]

Publication: 9 September 2006
MS 306-110

Figure F1. Ternary diagram showing nomenclature for principal components of whole sediment composition.

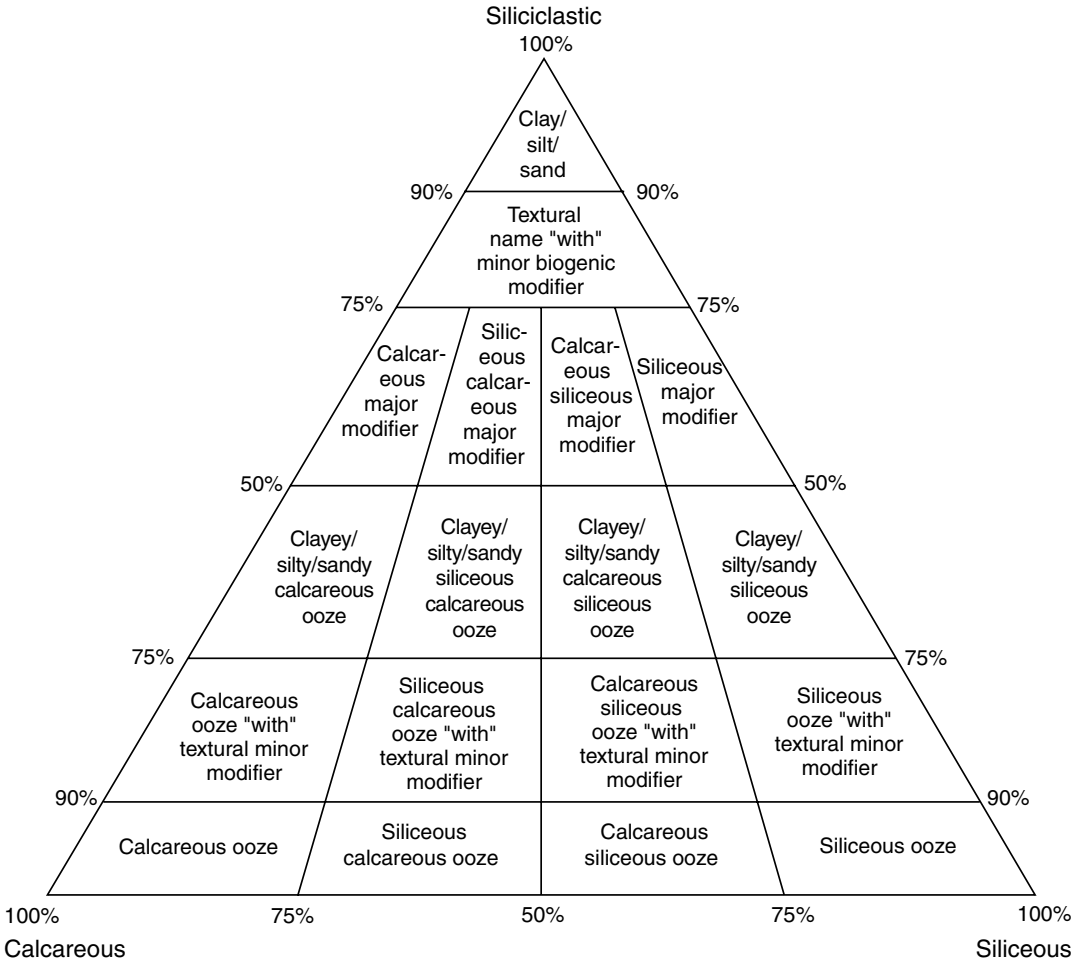

Figure F2. Grain-size classification scheme of Wentworth (1922).

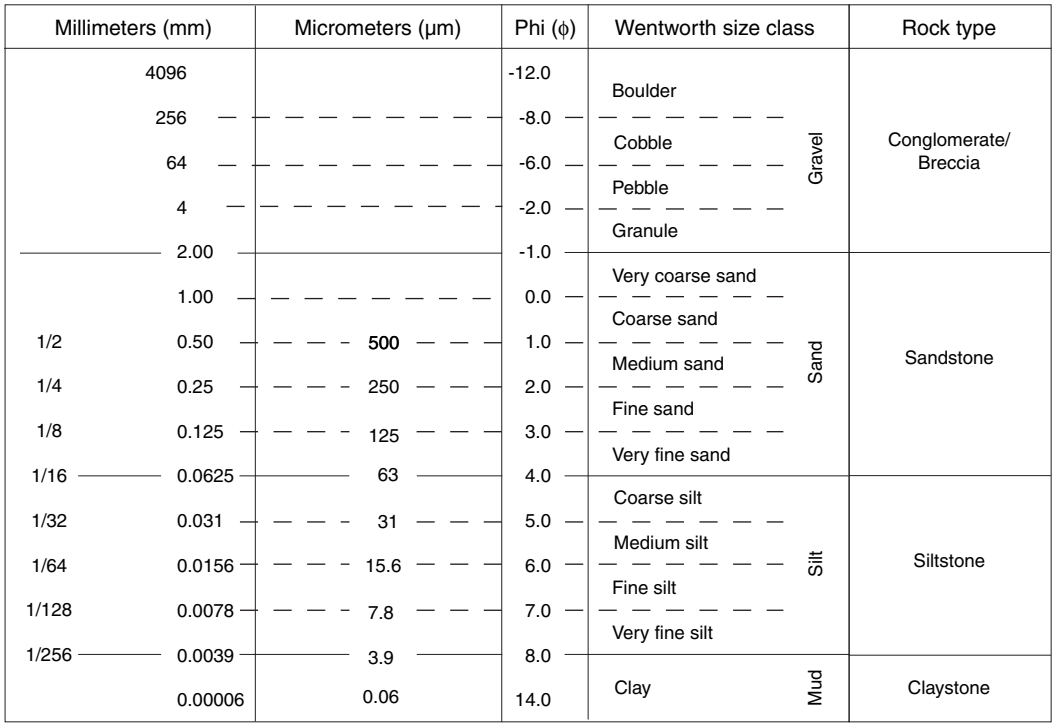

Figure F3. Ternary diagram showing nomenclature for siliciclastic sediment components based on grain size.

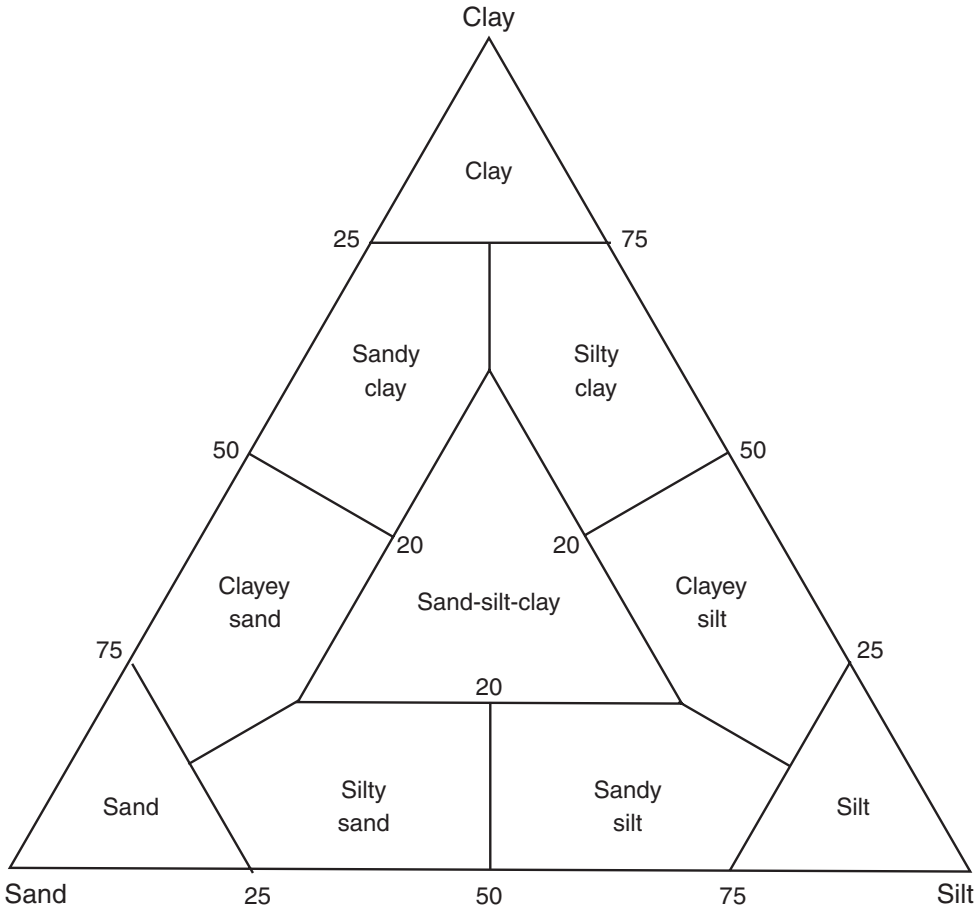

Figure F4. Example of an AppleCORE summary barrel sheet.

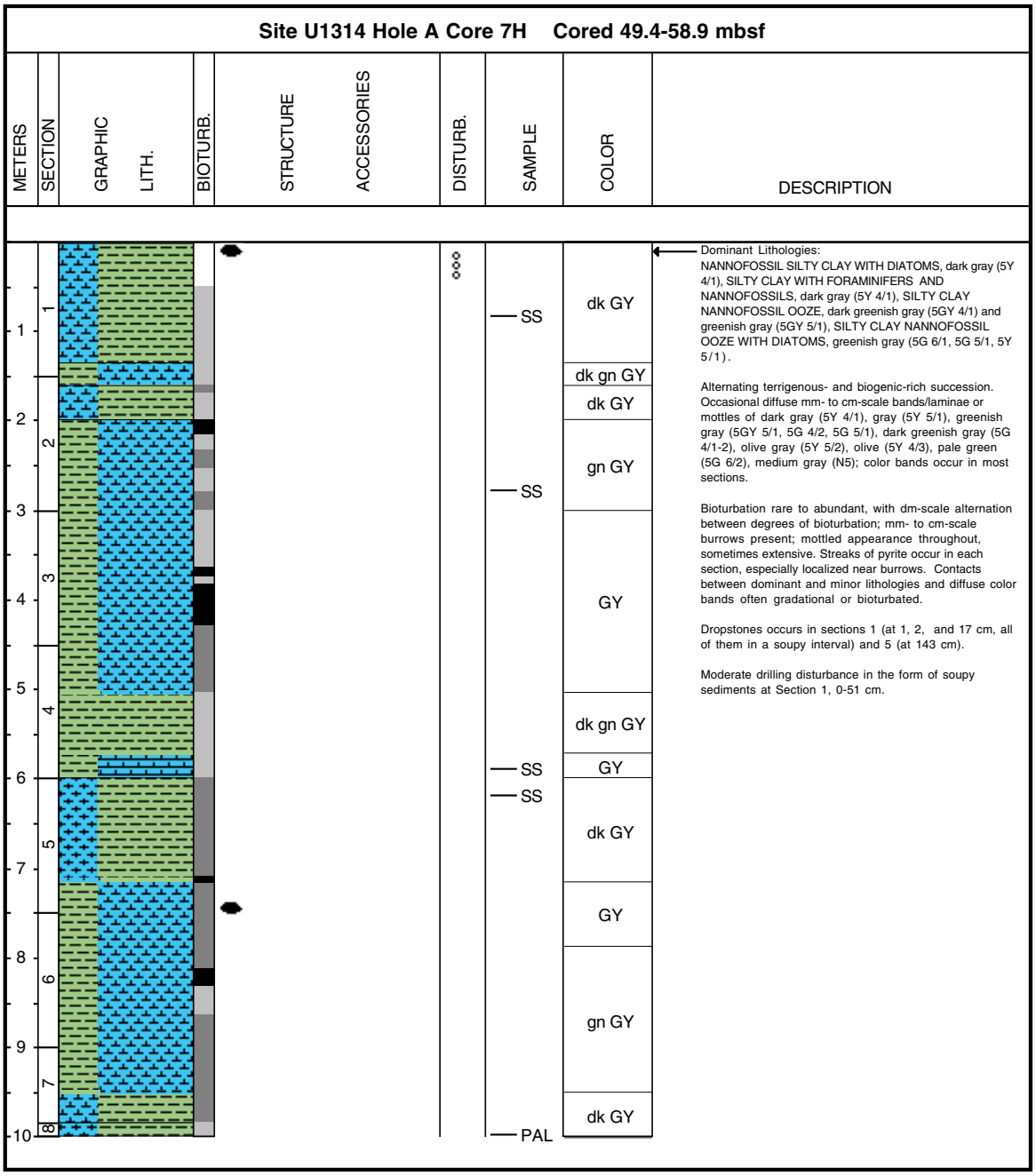

Figure F5. Key to symbols used for graphic lithologies.

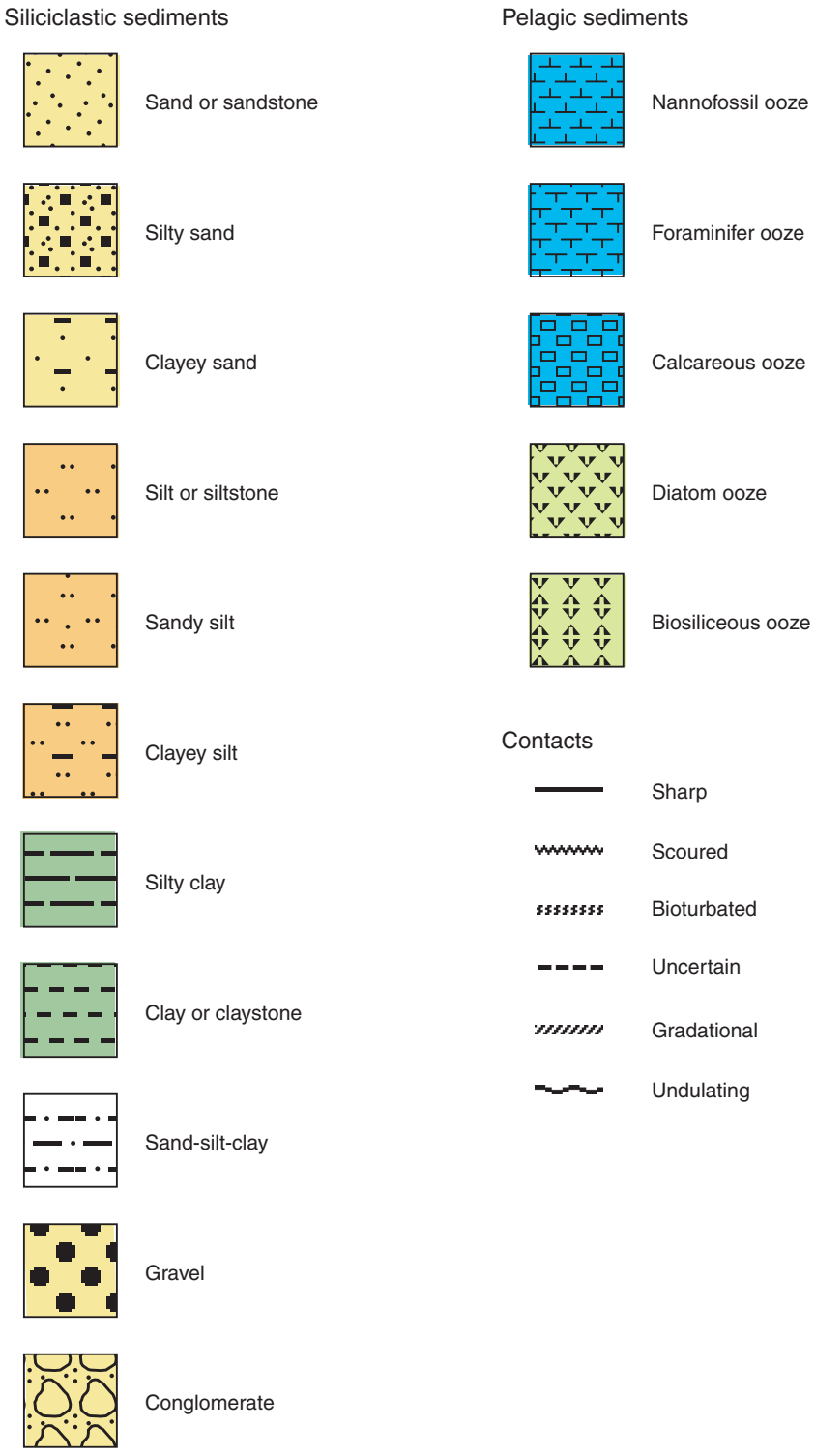

Figure F6. Key to other symbols used on the AppleCORE summary barrel sheets.

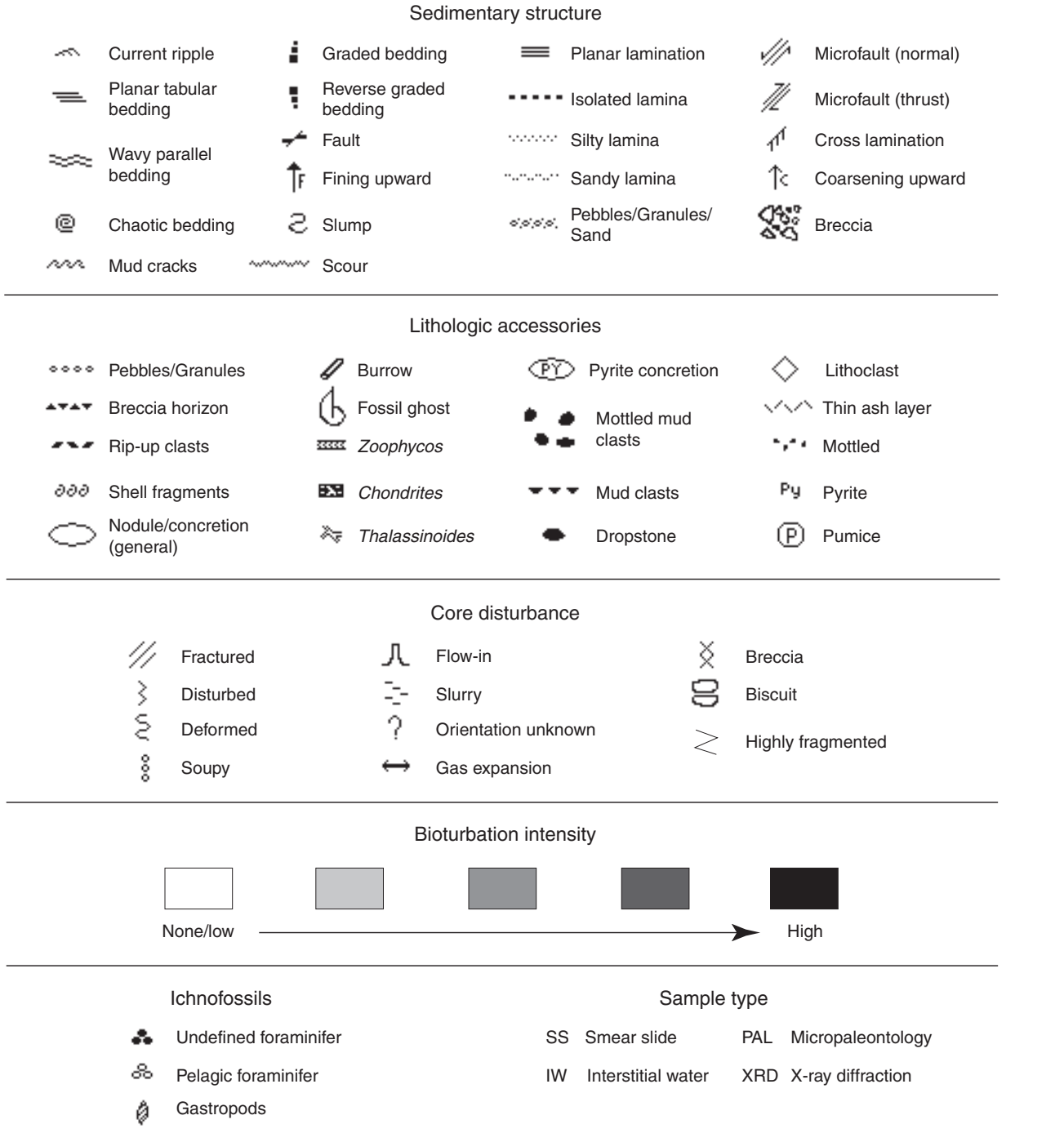

Figure F7. Key to ichnofabric index (bioturbation intensity) used during Expedition 306 (modified from Droser and Bottjer, 1991).

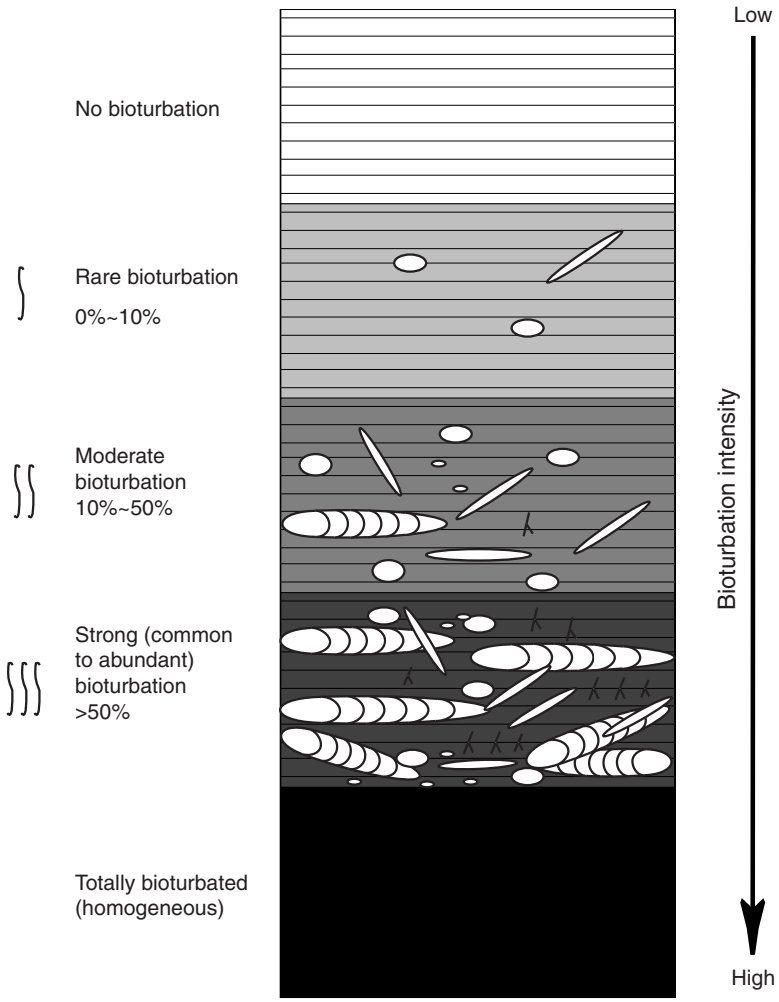

Figure F8. Correlation of geomagnetic polarity timescale (Cande and Kent, 1995), biostratigraphic zonation, and biohorizons used during Expedition 306. FO = first occurrence, FaO = first abundant occurrence, FcO = first common occurrence, FrO = first rare occurrence, LO = last occurrence, LcO = last common occurrence, Bm = morphotypic first appearance. s = sinistral, d = dextral.

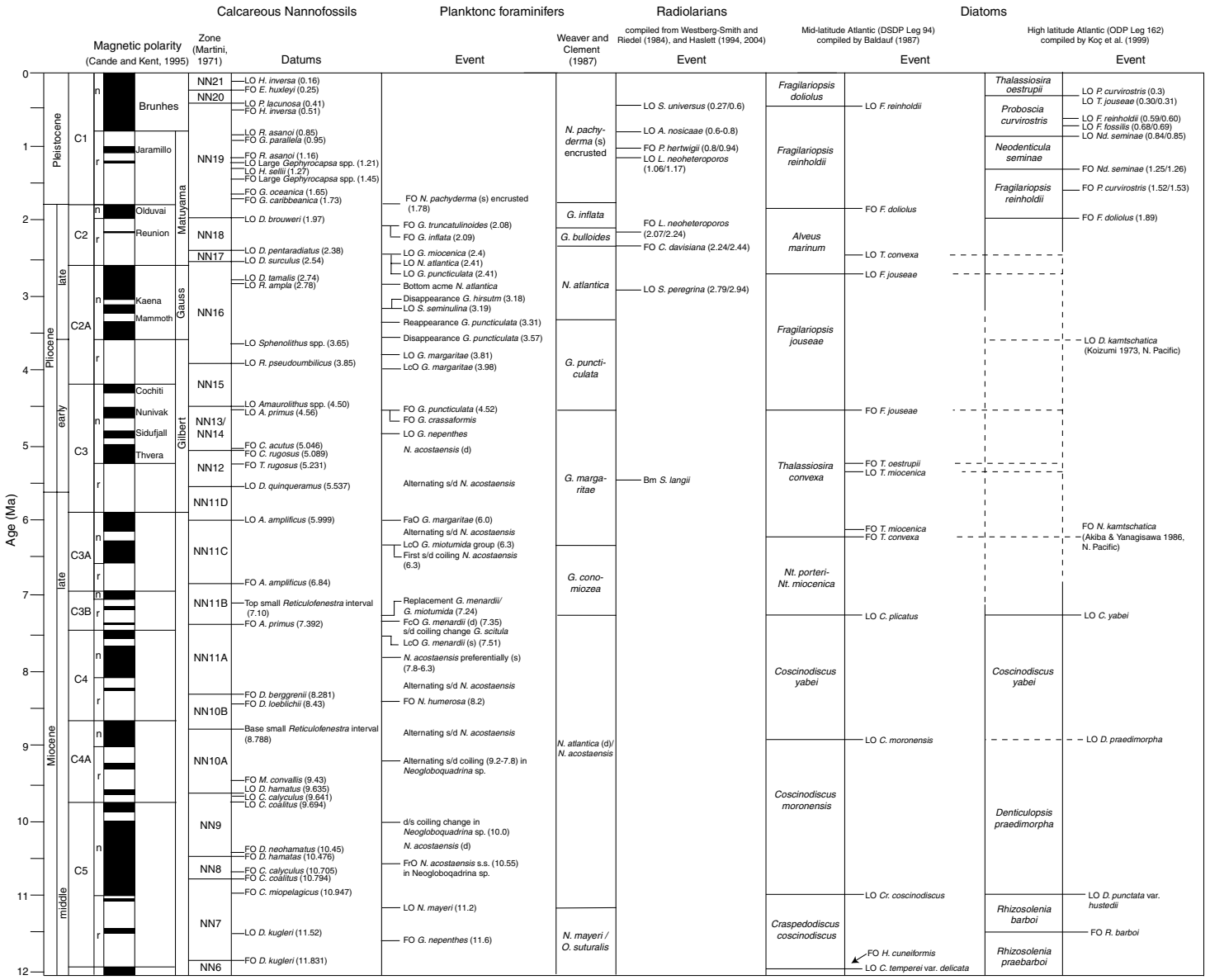

Figure F9. IODP paleomagnetic coordinate system for archive halves of core sections.

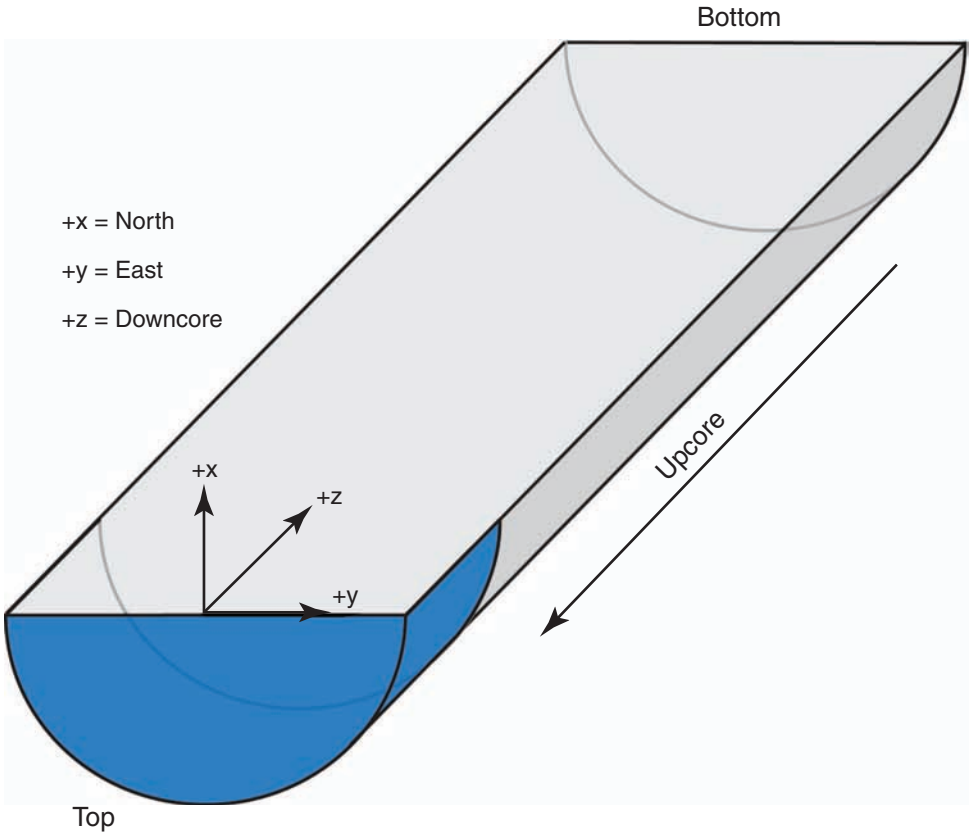

Figure F10. Comparison of TOC contents determined postcruise at the Alfred Wegener Institute (J. Hefter, unpubl. data, 2006) by two independent methods. Grey line = hypothetical 1:1 correlation.

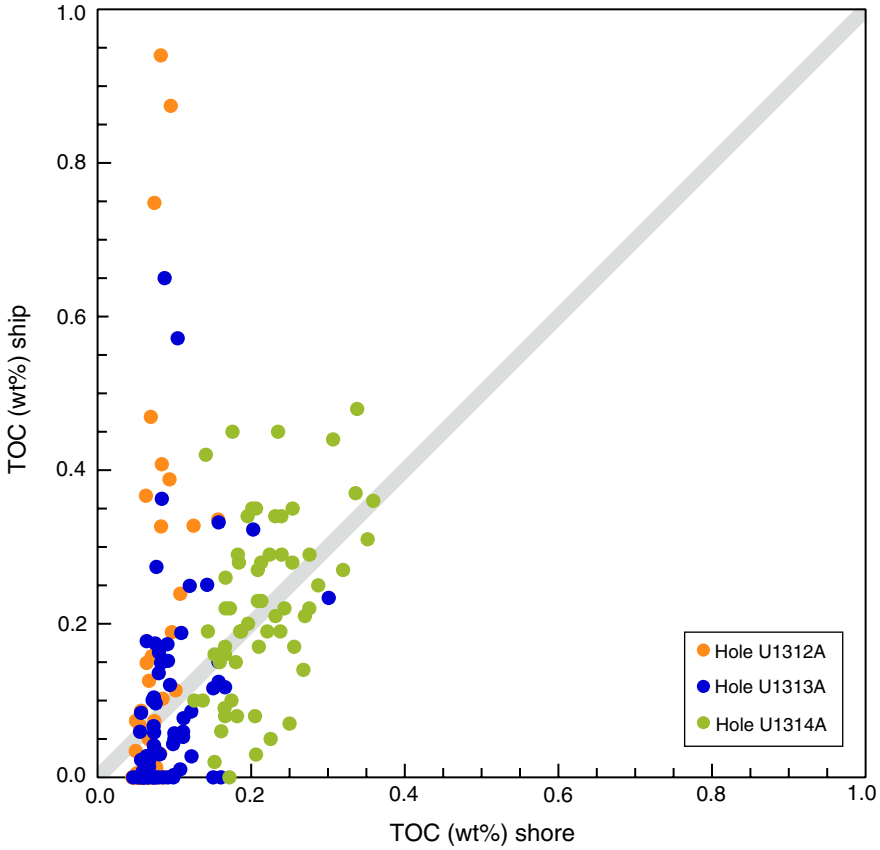

Figure F11. Configuration of the wireline logging tool strings used during IODP Expedition 306.

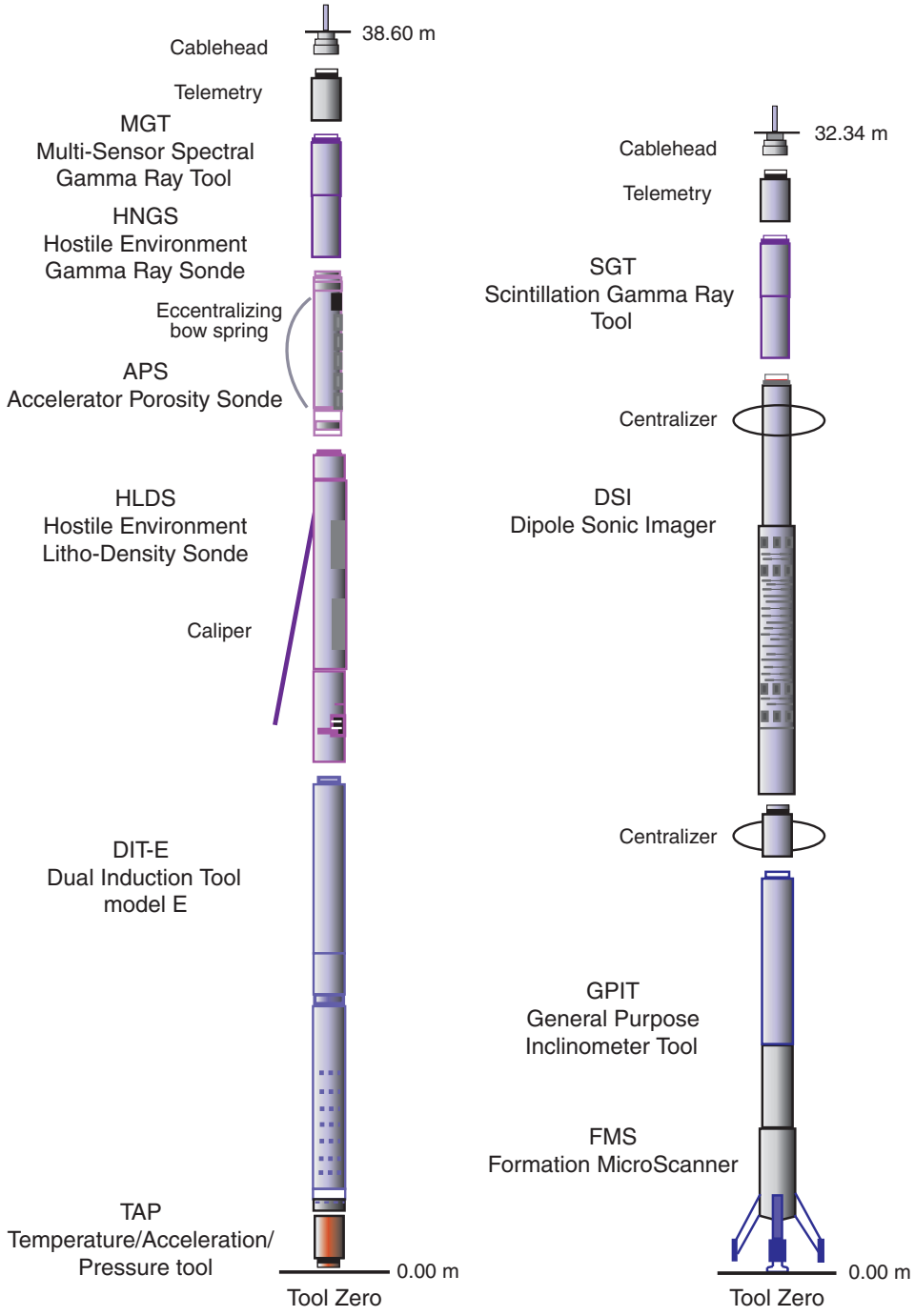

Table T1. Calcareous nannofossil events.

Species event	Zone (base)	Age (Ma)	Reference
LO *Helicosphaera inversa*	NN21	0.16	Sato et al., 1999
FO *Emiliania huxleyi*		0.25	Sato et al., 1999
LO *Pseudoemiliania lacunosa*	NN20	0.41	Sato et al., 1999
FO *Helicosphaera inversa*		0.51	Sato et al., 1999
LO *Reticulofenestra asanoi*		0.85	Sato et al., 1999
FO *Gephyrocapsa parallela*		0.95	Sato et al., 1999
FO *Reticulofenestra asanoi*		1.16	Sato et al., 1999
LO large *Gephyrocapsa* spp.	NN19	1.21	Sato et al., 1999
LO *Helicosphaera sellii*		1.27	Sato et al., 1999
FO large *Gephyrocapsa* spp.		1.45	Sato et al., 1999
FO *Gephyrocapsa oceanica*		1.65	Sato et al., 1999
FO *Gephyrocapsa caribbeanica*		1.73	Sato et al., 1999
LO *Discoaster brouweri*		1.97	Sato et al., 1999
LO *Discoaster pentaradiatus*	NN18	2.38	Sato et al., 1999
LO *Discoaster surculus*	NN17	2.54	Sato et al., 1999
LO *Discoaster tamalis*		2.74	Sato et al., 1999
LO *Reticulofenestra ampla*	NN16	2.78	Sato et al., 1999
LO *Sphenolithus* spp.		3.65	Raffi and Flores, 1995
LO *Reticulofenestra pseudoumbilicus*		3.85	Sato et al., 1999
LO *Amaurolithus primus*	NN13/NN14	4.56	Shackleton et al., 1995
LO *Ceratolithus acutus*		5.046	Backman and Raffi, 1997
FO *Ceratolithus rugosus*		5.089	Backman and Raffi, 1997
LO *Triquetrorhabdulus rugosus*	NN12	5.231	Backman and Raffi, 1997
LO *Discoaster quinqueramus*	NN11D	5.537	Backman and Raffi, 1997
LO *Amaurolithus amplificus*	NN11C	5.999	Backman and Raffi, 1997
FO *Amaurolithus amplificus*		6.84	Backman and Raffi, 1997
Top small *Reticulofenestra* interval	NN11B	7.10	Backman and Raffi, 1997
FO *Amaurolithus primus*		7.392	Backman and Raffi, 1997
FO *Discoaster berggrenii*	NN11A	8.281	Backman and Raffi, 1997
FO *Discoaster loeblichii*	NN10B	8.43	Raffi and Flores, 1995
Base small *Reticulofenestra* interval		8.788	Backman and Raffi, 1997
FO *Minylitha convallis*	NN10A	9.43	Raffi and Flores, 1995
LO *Discoaster hamatus*		9.635	Backman and Raffi, 1997
LO *Catinaster calyculus*		9.641	Backman and Raffi, 1997
LO *Catinaster coalitus*	NN9	9.694	Backman and Raffi, 1997
FO *Discoaster neohamatus*		10.45	Backman and Raffi, 1997
FO *Discoaster hamatus*		10.476	Backman and Raffi, 1997
FO *Catinaster calyculus*	NN8	10.705	Backman and Raffi, 1997
FO *Catinaster coalitus*		10.794	Backman and Raffi, 1997
LO *Coccolithus miopelagicus*		10.947	Backman and Raffi, 1997
LO *Discoaster kugleri*	NN7	11.52	Backman and Raffi, 1997
FO *Discoaster kugleri*		11.831	Backman and Raffi, 1997

Notes: LO = last occurrence, FO = first occurrence.

Table T2. Planktonic foraminifer stratigraphic events.

Species event	Age (Ma)	Polarity interval	Reference	Region
FO *Neogloboquadrina pachyderma* (s) (encrusted)	1.78	Top Olduvai	Weaver and Clement, 1987	N. Atlantic
FO *Globorotalia truncatulinoides*	2.08	Base Olduvai	Spezzaferri, 1998	N. Atlantic
FO *Globorotalia inflata*	2.09	Base Olduvai–Reunion	Weaver and Clement, 1987; Lourens et al., 1996	N. Atlantic, Mediterranean
LO *Globorotalia miocenica*	2.4	Reunion–Gauss/Matuyama	Weaver and Clement, 1987	N. Atlantic
LO *Neogloboquadrina atlantica*	2.41	Reunion–Gauss/Matuyama	Weaver and Clement, 1987; Lourens et al., 1996	N. Atlantic, Mediterranean
LO *Globorotalia puncticulata*	2.41	Reunion–Gauss/Matuyama	Weaver and Clement, 1987; Lourens et al., 1996	N. Atlantic, Mediterranean
Disappearance *Globorotalia hirsuta*	3.18	Base Kaena–top Mammoth	Weaver and Clement, 1987	N. Atlantic
LO *Sphaeroidinellopsis seminulina*	3.19	Base Kaena–top Mammoth	Weaver and Clement, 1987; Lourens et al., 1996	N. Atlantic, Mediterranean
Reappearance *Globorotalia puncticulata*	3.31		Lourens et al., 1996	Mediterranean
Disappearance *Globorotalia puncticulata*	3.57		Lourens et al., 1996	Mediterranean
LO *Globorotalia margaritae*	3.81	Base Gauss–Cochiti	Weaver and Clement, 1987; Lourens et al., 1996	N. Atlantic, Mediterranean
LcO *Globorotalia margaritae*	3.98	Base Gauss–Cochiti	Weaver and Clement, 1987; Lourens et al., 1996	N. Atlantic, Mediterranean
FO *Globorotalia puncticulata*	4.52	Nunivak	Weaver and Clement, 1987; Lourens et al., 1996	N. Atlantic, Mediterranean
FO *Globorotalia crassaformis*		Nunivak	Weaver and Clement, 1987	Mediterranean
LO *Globgerina nepenthes*	4.8–4.89	Sidufjall	Weaver and Clement, 1987	Mediterranean
FcO *Globorotalia margaritae*	6	C3A.1n	Sierro et al., 1993	N. Atlantic
Alternating (s/d) *Neogloboquadrina acostaensis*	6–6.3	Below C3A.1n	Hodell et al., 2001	N. Atlantic
LcO *Globorotalia miotumida* group	6.3	Below C3A.1n		
First coiling change *Neogloboquadrina acostaensis* (s/d)	6.3	Below C3An.1n	Sierro et al., 1993, 2001; Hilgen et al., 1995; Krijgsman et al., 1995	Atlantic, Mediterranean
Replacement *Globorotalia menardii*/ *Globorotalia miotumida*	7.24	Below C3Bn	Sierro et al., 1993; Krijgsman et al., 1995	Atlantic, Mediterreanean
FcO *Globorotalia menardii* (d)	7.35	Below C3Br.1n	Sierro et al., 1993; Krijgsman et al., 1995	Atlantic
Coiling change *Globorotalia scitula* (s/d)			Sierro et al., 1993	Atlantic
LcO *Globorotalia menardii* (s)	7.51	Below C3Br.2n	Krijgsman et al., 1995; Sierro et al., 1993	Mediterranean, Atlantic
Neogloboquadrina acostaensis preferentially (s)	6.3–7.8		Krijgsman et al., 1999	Mediterranean
FO *Neogloboquadrina humerosa*	8.2	C4r.2r	Spezzaferri, 1998	N. Atlantic
Alternating (s/d) in *Neogloboquadrina* sp.	7.8–9.2		Krijgsman et al., 1999	Mediterranean
Coiling in *Neogloboquadrina* (d/s)	10	Top C5n.2n	Hilgen et al., 2000	Mediterranean
FrO *Neogloboquadrina acostaensis* s.s.	10.55	C5n.2n	Hilgen et al., 2000	Mediterranean
LO *Neogloboquadrina mayeri*	11.2	Top C5r.2r	Hilgen et al., 2000	Mediterranean
FO *Globigerina nepenthes*	11.6	C5r.3r	Spezzaferri, 1998	N. Atlantic

Notes: FO = first occurrence, LO = last occurrence, LcO = last common occurrence, FcO = first common occurrence, FrO = first rare occurrence. d = dextral, s = sinistral.

Table T3. Analytical methods and precisions for interstitial water geochemical measurements.

Parameter	Precision (%)	Method
Cl^-	0.1	Titration with $AgNO_3$
SO_4^{2-}	2.3	Ion chromatography
NH_4^+	1.7	Spectrophotometer
Na^+	3.1	ICP-AES
K^+	10.8	ICP-AES
Mg^{2+}	8.8	ICP-AES
Ca^{2+}	6.2	ICP-AES
Li^+	2.6	ICP-AES
Sr^{2+}	3.6	ICP-AES
Ba^{2+}	15.8	ICP-AES
Mn^{2+}	2.8	ICP-AES
Fe^{2+}	4.5	ICP-AES
H_3BO_3	4.8	ICP-AES
H_4SiO_4	5	ICP-AES

Note: ICP-AES = inductively coupled plasma–atomic emission spectroscopy.

Table T4. Measurements and specifications for wireline tools.

Tool string	Tool	Measurement	Sampling interval (cm)	Approximate vertical resolution (cm)
Triple combination	MGT*	Spectral gamma ray		15
	HNGS‡	Spectral gamma ray	15	51
	APS	Porosity	5 and 15	43
	HLDT	Bulk density	2.5	38
	DIT-E	Resistivity	15	200/150/76
	TAP	Temperature	1 per s	NA
		Tool acceleration	4 per s	NA
		Pressure	1 per s	NA
Formation MicroScanner (FMS)-sonic combination	NGT	Spectral gamma ray	15	46
	GPIT	Tool orientation	0.25 and 15	NA
	FMS	Microresistivity	0.25	0.5
	DSI/SDT/LSS/BHC	Acoustic velocity	15	107

Notes: All tool and tool string names (except the TAP and MGT tools) are trademarks of Schlumberger. For additional information about tool physics and use, consult IODP–USIO Science Services, LDEO, at **iodp.ldeo.columbia.edu/TOOLS_LABS/tools.html**. See Table **T5** for explanations of acronyms used to describe tool strings and tools. * = not included in each logging run. NA = not applicable.

Table T5. Acronyms and units for wireline tools.

Tool	Output	Tool name/Explanation of output	Unit
APS		Accelerator Porosity Sonde	
	APLC	Near array porosity (limestone calibrated)	%
	SIGF	Formation capture cross section (S_f)	Capture units
	STOF	Tool standoff (computed distance from borehole wall)	Inches
DIT-E		Dual Induction Tool model E	
	IDPH	Deep induction resistivity	Ω·m
	IMPH	Medium induction resistivity	Ω·m
	SFLU	Spherically focused resistivity	Ω·m
DSI		Dipole Sonic Imager	
	DTCO	Compressional wave delay time (Dt)	ms/ft
	DTSM	Shear wave delay time (Dt)	ms/ft
	DTST	Stoneley wave delay time (Dt)	ms/ft
FMS		Formation MicroScanner	
	C_1, C_2	Orthogonal hole diameters	Inches
	P1AZ	Pad 1 azimuth	Degrees
		Spatially oriented resistivity images of borehole wall	
GPIT		General Purpose Inclinometer Tool	
	DEVI	Hole deviation	Degrees
	HAZI	Hole azimuth	Degrees
	Fx, Fy, Fz	Earth's magnetic field (three orthogonal components)	Degrees
	Ax, Ay, Az	Acceleration (three orthogonal components)	m/s^2
HLDT		Hostile Environment Litho-Density Tool	
	RHOM	Bulk density	g/cm^3
	PEFL	Photoelectric effect	b/e^-
	LCAL	Caliper (measure of borehole diameter)	Inches
	DRH	Bulk density correction	g/cm^3
HNGS		Hostile Environment Gamma Ray Sonde	
	HSGR	Standard (total) gamma ray	gAPI
	HCGR	Computed gamma ray (HSGR minus uranium contribution)	gAPI
	HFK	Potassium	wt%
	HTHO	Thorium	ppm
	HURA	Uranium	ppm
NGT		Natural Gamma Ray Spectrometry Tool	
	SGR	Standard total gamma ray	gAPI
	CGR	Computed gamma ray (SGR minus uranium contribution)	gAPI
	POTA	Potassium	wt%
	THOR	Thorium	ppm
	URAN	Uranium	ppm
MGT		Multi-Sensor Spectral Gamma Ray Tool	
	GR	Total gamma radiation	gAPI
TAP		Temperature/Acceleration/Pressure tool	°C, m/s^2, psi

Note: All tool and tool string names (except the TAP tool) are trademarks of Schlumberger. For the complete list of acronyms used in IODP and for additional information about tool physics and use, consult IODP–USIO Science Services, LDEO, at **iodp.ldeo.columbia.edu/TOOLS_LABS/tools.html.**